SYNTHESIS AND CHARACTERIZATION OF TIN-DOPED CADMIUM OXIDE NANOPARTICLES FOR SOLAR CELL APPLICATION

Nancy Jepchumba Kiprotich

A Thesis submitted in Partial Fulfilment of the Requirements for the Degree of Master of Science in Physics of Murang'a University of Technology

August, 2025

DECLARATION

Student Declaration

I hereby declare that this Thesis is my original work and to the best of my knowledge has not been presented for a degree award in this or any other university. I understand what plagiarism is and I am aware of the University's policy in this regard. I understand that any false claim in respect of this work shall result in disciplinary action in accordance with the University Anti-Plagiarism Policy.

_____ _____

Nancy Jepchumba Kiprotich Date
AS402/5108/2023

Supervisors' Approval

The undersigned certify that they have read and hereby recommended for acceptance of Murang'a University of Technology a thesis entitled **"Synthesis and Characterization of Sn Doped CdO Nanoparticles for Solar Cell Application"**.

_____ _____

Dr. John Njagi Nguu, Date
Department of Physical and Biological Sciences,
Murang'a University of Technology.

_____ _____

Dr. Peter Njoroge Waithaka, Date
Department of Physical and Biological Sciences,
Murang'a University of Technology.

DEDICATION

This thesis is dedicated to my mother Martina Talai, who continuously prayed for me, my sister Dr Sharon Kiprotich, and brother David Rotich, who gave me financial support and encouragement throughout the process, my children Zibiah Jepkemoi and Hiram Kipruto, who gave me ample time in completing the study, and finally to my best friend Cornelius Kibet, who continuously reminded me about the work plan.

ACKNOWLEDGEMENT

I thank God for His unconditional love and the sufficient Grace that enabled me to complete this research successfully.

This research is made possible thanks to the SG-NAPI award supported by the German Ministry of Education and Research, BMBF through UNESCO-TWAS for the funding.

Gratitude to my supervisors Dr. Njagi John and Dr. Peter Waithaka for their continued guidance throughout the research study and to the School of Pure, Applied and Health sciences (SPAHS); Prof. Sylvia Opiyo, Dr. Sharon Kiprotich and the technical staff, God bless you for the immense support.

Sincere thanks go to Murang'a University of Technology for giving me the chance to pursue my studies and, more so, for facilitating the required resources and equipment that enabled the successful completion of my research.

Finally, thanks to my course mates, Nimrod Gitonga, Ayabei Shadrack, Bethwel Kiprotich, Collins Wakavu and James Waweru for their moral support throughout the study.

ABSTRACT

The rising demand for clean, sustainable energy globally has led researchers to research on possible improvements on existing materials in photovoltaic applications. Cadmium oxide (CdO), an n-type semiconductor, containing a large bandgap, has the prospective features for solar cell application because of its high visible band transparency, electroconductivity, and stability. This work aimed at synthesizing and characterizing tin (Sn)-doped CdO nanoparticles (CdO: Sn NPs) using wet chemical process at varying ratios of mercaptopropionic acid (MPA), tin (Sn) doping concentration and different calcination temperatures to investigate the effects on the structural and optical properties. X-ray diffraction (XRD) analysis ascertained the retention of the face-centred cubic structure of CdO, indicating the successful incorporation of Sn. Increase in calcination temperature brought enhancement in the Crystallinity, where the optimum crystallite size was 27.98nm at 500 °C. The best optical and structural properties were, however, realized at a calcination temperature of 350°C, after which defect density and agglomeration of the particles became high. The ratio of MPA capping was significant in the customization of nanoparticles. The ratios of 2 ml MPA enabled the crystals to be grown as well-defined and with low defects, giving a low ratio of strain and dislocations, whereas the ratio values of 2.5-3.0 ml interfered with the crystals, thus resulting in a higher ratio of strain and dislocations. It was confirmed that the successful bonds between the MPA functional groups were formed through the Fourier-transform infrared spectroscopy (FTIR) technique, where characteristic Cd-O, C-O, O-H, and S-H resonances became more distinct with increments of at an equivalent ratio. Optical characterizations were carried out under UV-Visible spectroscopy, and the absorption edge was nearly redshifted upon the addition of Sn and MPA. At high levels of doping and standard capping, the optical bandgap varied between 5.5 eV and 1.812 eV. Analysis using photoluminescence (PL) showed the existence of a number of emission lines relating to the oxygen vacancies and surface states. The surface passivation was the greatest, and non-radiative recombination was lowest, as the sample with 2ml of MPA-covering resulted in the greatest PL intensity. Therefore, nanoparticles with the highest performance were acquired at 2 mL concentration of MPA, 1.5% Sn-doping, and 350°C calcination. The optimized parameters produced nanoparticles of very fine structural with tuneable optical properties, hence they can be considered as the most likely candidates to serve as photoanode materials in cheap and clean solar cells. This study offers new information on the synthesis of semiconductor materials in the engineering of new energy transducers.

TABLE OF CONTENTS

DECLARATION ..... **ii**
DEDICATION ..... **iii**
ACKNOWLEDGEMENT ..... **iv**
ABSTRACT ..... **v**
LIST OF TABLES ..... **ix**
LIST OF FIGURES ..... **x**
ACRONYMS AND ABBREVIATIONS ..... **xii**
DEFINITION OF OPERATIONAL TERMS ..... **xiii**
CHAPTER ONE: INTRODUCTION **1**
1.1 Background of the study 1
1.2 Statement of the problem 5
1.3 Objectives of the study 6
1.3.1 General objective 6
1.3.2 Specific objectives 6
1.4 Research Questions 6
1.5 Significance of the study 7
1.6 Scope of the study 7
1.7 Contribution of the study 7
1.8 Organization of the Thesis 8
CHAPTER TWO: LITERATURE REVIEW **10**
2.1 Introduction 10
2.2 Sources of Energy 10
2.3 Classification of solar cells 11
2.3.1 First-generation solar cell 11
2.3.2 Second generation solar cells 12
2.3.3 Third-generation solar cells 12
2.4 Properties of CdO 13
2.5 Effects of Capping Agent 15
2.6 Effects of Tin (Sn) Doping 15
2.7: Effects of Calcination Temperature 16
2.8: Method of Synthesizing Nanoparticles 16
2.9: Chapter Summary 17
CHAPTER THREE: MATERIALS AND METHODS **18**
3.1 Introduction 18
3.2 Materials 18
3.2.1 Reagents 18
3.2.2 Apparatus 18

3.3 Methods 19
3.3.1 Synthesis of CdO Nanoparticles 19
3.3.2 Capping of CdO nanoparticles with Mercaptopropionic Acid (MPA) 19
3.3.3 Tin Doping of MPA-Capped CdO Nanoparticles 20
3.3.4 Calcination Process 20
3.4 Analytical Techniques 21
3.4.1 X-Ray diffraction (XRD) 21
3.4.2 Fourier transform infrared spectroscopy (FTIR) 22
3.4.3 Ultra-Violet visible spectrometer (UV-Vis) 24
3.4.4 Photoluminescence Spectroscopy (PL) 26
3.5 Chapter Summary 26
CHAPTER FOUR: RESULTS AND DISCUSSION 28
4.1 Introduction 28
4.2. Investigating the effects of capping ratio on the structural and optical properties of Mercaptopropionic acid-capped cadmium oxide nanoparticles 28
4.2.1 X-ray Diffraction (XRD) Analysis 28
4.2.2 UV-Vis 31
4.2.3 Bandgap analysis 32
4.2.4 Photoluminescence 34
4.2.5 FTIR Analysis 36
4.3 Effects of Tin doping concentration on the structural and optical properties of Cadmium oxide nanoparticles 38
4.3.1 XRD analysis 38
4.3.2 UV-Vis analysis 42
4.3.3 Band gap analysis 43
4.3.4 Photoluminescence (PL) analysis 45
4.4 Effects of varying calcination temperature on the structural, and optical properties of tin-doped cadmium oxide nanoparticles. 47
4.4.1 XRD Results 47
4.4.2 Photoluminescence Analysis 51
4.4.3 FTIR Analysis 53
4.4.4 Optical Analysis 55
4.5 Chapter Summary 58
CHAPTER FIVE: CONCLUSION AND RECOMMENDATIONS 60
5.1 Conclusion 60
5.2 Recommendations 62
5.2.1 Recommendations for Policy 62
5.2.2 Recommendation for future work 62
REFERENCES 64

APPENDICES 74

LIST OF TABLES

Table 2.1: Output power and conversion efficiencies of the crystalline solar cell. 13
Table 4.1: Showing the crystallite sizes of MPA-capped CdO NPs ……30
Table 4.2: Showing average d spacing, lattice parameters, strain and dislocation density of MPA capped CdO NPs 30
Table 4.3: Band gap values of MPA-capped CdO NPs 34
Table 4.4: Emission wavelengths and relative intensities of MPA capped CdO NPs 36
Table 4.5: Tabulated crystallite sizes D (nm) using plane (111) for pure CdO and Sn-doped CdO 41
Table 4.6: Structural parameters for pure CdO and Sn-doped CdO 42
Table 4.7: Summarized table showing absorption edge and bandgap energies for different concentrations of tin doping 45
Table 4.8: Showing Summary of tin doping concentration, emission wavelength and relative intensity for pure and doped CdO 47
Table 4.9: Showing the crystallite sizes of Sn: CdO NPs at varying calcination temperatures. 49
Table 4.10: Showing lattice parameters, d spacing, strain, and dislocation of synthesized Sn: CdO NPs at varying calcination temperatures 51
Table 4.11: Emission wavelengths and relative intensities of peaks at varying calcination temperatures 53
Table 4.12: Showing extrapolated bandgaps of Sn-CdO NPs at different calcination temperatures..... 58

LIST OF FIGURES

Figure 1.1: Non-renewable sources of energy 1
Figure 1.2: Renewable sources of energy 2
Figure 1.3: Diagram illustrating Dye sensitized solar cell 3
Figure 2.1: Generation of solar cell technologies 13
Figure 2.2: Crystal structure of cadmium oxide 15
Figure 2.3: Preparation of cadmium oxide nanoparticles 17
Figure 3.1: Preparation of MPA capped cadmium oxide nanoparticles doped with tin through precipitation by reflux method. 21
Figure 3.2: ARL EQUINOX X-ray diffractometer at Murang'a University of Technology. 22
Figure 3.3: Shimadzu IR Spirit FT-IR model at Murang'a University of Technology 24
Figure 3.4: Evolution one plus UV-Vis spectroscopy at Murang'a University of Technology 25
Figure 3.5: SP-LF97 model PL Spectroscopy at Murang'a University of Technology 26
Figure 4.1: The XRD patterns of MPA-capped and uncapped CdO nanoparticles prepared with different concentrations of MPA. 29
Figure 4.2: The evolution of absorbance spectra of CdO nanoparticles for different concentrations of the capping agent. 31
Figure 4.3: Tauc's plot for capped cadmium oxide nanoparticles with different concentrations of mercaptopropionic acid (MPA). 33
Figure 4.4: (Left) PL spectra of MPA capped CdO NPs and (Right) Gaussian deconvolution of 2.0 ml MPA capped CdO NPs. 35
Figure 4.5: FTIR spectra of MPA-capped CdO NPs at different capping ratios. 37
Figure 4.6: XRD spectra for the pure CdO and doped CdO with various concentration of tin prepared using wet chemical technique. 39
Figure 4.7: The XRD major intensity peaks for varying levels of tin for (111) plane synthesized using wet chemical process. 40
Figure 4.8: The evolution of absorbance spectra of different tin doping concentrations. 43
Figure 4.9: Tauc's plot (a) and band gap energies of the NPs (b) for different Sn doping concentrations. 44
Figure 4.10: (a) Photoluminescence emission spectra of tin doped CdO and (b) undoped CdO. 46
Figure 4.11: Deconvoluted graph of 1.5% Sn doping 46

Figure 4.12: XRD pattern of synthesized Sn: CdO NPs at varying calcination temperatures. 48
Figure 4.13: PL spectra showing Sn- CdO NPs calcined at different temperatures (a) and Gaussian deconvolution at 350 0C (b) 52
Figure 4.14: FTIR spectra of Sn- CdO NPs at different calcination temperatures 54
Figure 4.15: Absorbance spectra of Sn- CdO NPs calcined at different temperatures 56
Figure 4.16: Tauc's plot and band of CdO: Sn NPs at different calcination temperatures 57

ACRONYMS AND ABBREVIATIONS

a.u	Arbitrary unit
$C_3H_6O_2S$	Mercaptopropionic acid
Cd $(CH_3CO_2)_2$	Cadmium acetate di-hydrate
CdO	Cadmium Oxide
CdO:Sn	Tin-doped cadmium oxide
eV	Electron volts
FTIR	Fourier transform infrared spectroscopy
JCPDs	Joint committee on powder diffraction standards
MPA	Mercaptopropionic acid
NaOH	Sodium hydroxide
PCE	Power conversion efficiency
PL	photoluminescence
PV	Photovoltaic
Rpm	Revolution per minute
$SnCl_2$	Tin chloride
UV	Ultra-violet
XRD	X-ray diffraction

DEFINITION OF OPERATIONAL TERMS

Annealing -The use of heat to treat material or compound at a high temperature and slowly cooled at a control rate to remove stress, or to alter its structural, chemical and physical properties of material.

Bandgap energy – This is the distance in energy level separating the valence band and the conduction band in metal, semiconductors and insulators.

Capping agents – they are molecules that inhibit overgrowth of nanoparticles and prevent coagulation during colloidal synthesis.

Characterize -The application of scientific methods such as microscopy to interpret the composition of the material or compound.

Crystal size -is the physical dimension of individual crystal in material. It is used to describe the distribution of crystal in the material, and to analyse the physical, chemical and mechanical parameters of crystalline substances.

Doping - refers to the incorporation of foreign material into the lattice crystal of the host material to modify its structural, electrical, optical and morphological properties.

Photoanode - is a component of a solar cell responsible for the production of electrical energy from light energy.

Passivation- refers to a process where a material becomes less reactive by forming a protective layer on its surface.

Quantum confinement-is a phenomenon that occurs when the size of a semiconductor material is reduced to the nanoscale typically below the exciton Bohr radius, causing the movement of charge carriers (electrons and holes) to be restricted in one or more dimensions.

Synthesis -It is a process of obtaining a compound, material or a substance by combining individual elements or molecules in a systematic manner.

CHAPTER ONE

INTRODUCTION

1.1 Background of the study

Energy consumption has continued to rise due to civilization (Prakash *et al.*, 2021). The energy catastrophe has raised attention in the development of clean, renewable energy sources (Langat *et al.,* 2022). One of the key worries is the contribution of rising carbon dioxide emissions and diminishing fossil fuel inventories to global warming (Sharma *et al.,* 2015). Energy sources are classified into two; non-renewable and renewable energy sources as shown in Figure 1.1 and 1.2.

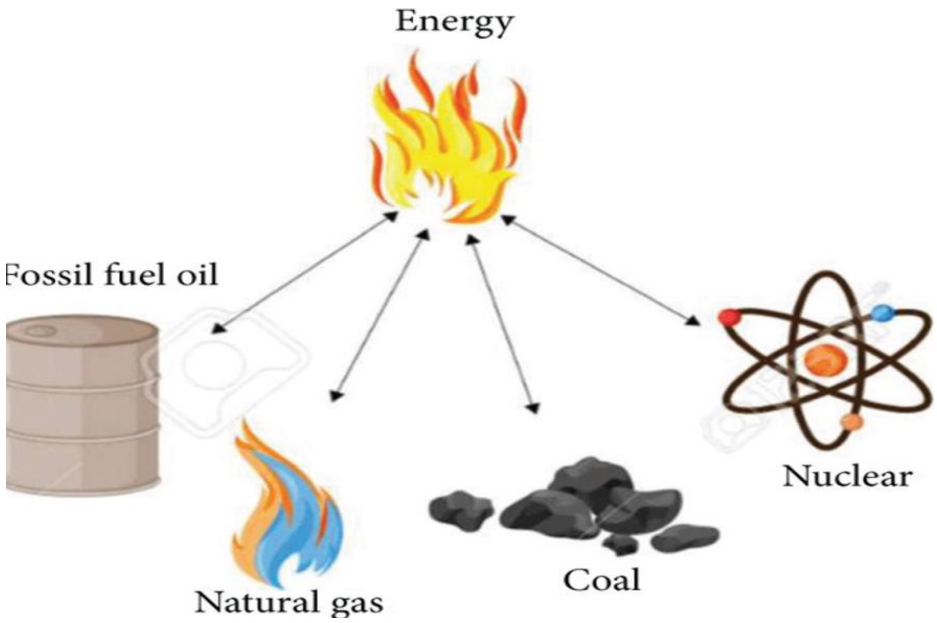


Figure 1.1: Non-renewable sources of energy (Bekele & Sintayehu, 2022)

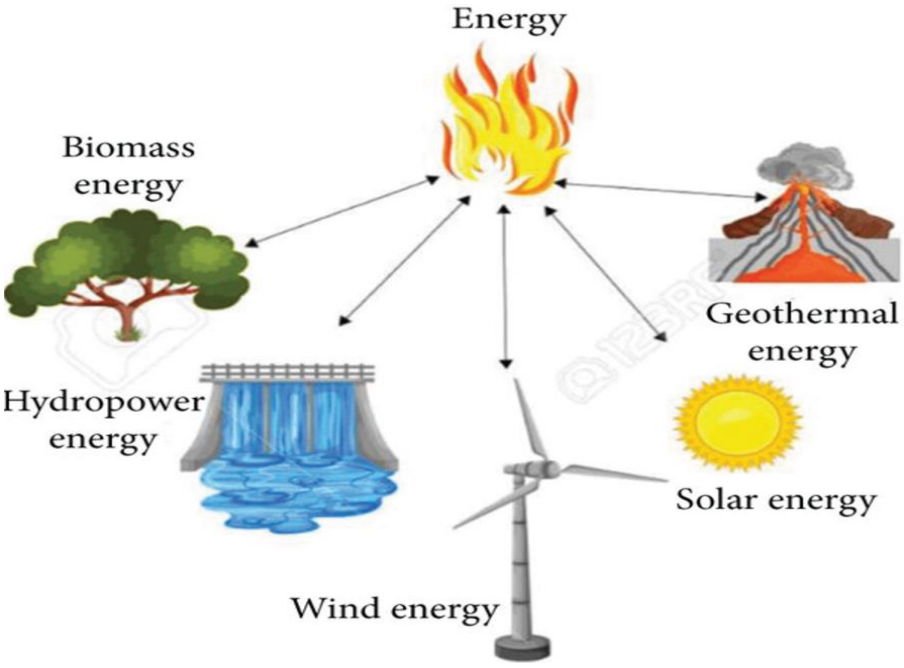


Figure 1.2: Renewable sources of energy (Bekele & Sintayehu, 2022)

More power use is anticipated in the future to support human progress. There is a lot of promise for using photoanodes in photovoltaic solar cells as an environmentally and financially sustainable renewable energy source (Rathore *et al.,* 2021). A photovoltaic solar cell is a device that uses the photovoltaic effect to generate electrical energy by converting light energy(Lu, 2023). Layers of a semi-conducting substance are present in every photovoltaic cell (PV). When light hits the cell, electricity is created across the semiconductor's layers due to electric field (Rathore *et al.,* 2021). The amount of electricity contained in the cell is dependent on the intensity of the light that strikes it. The direct current (DC) can be changed into an alternating current (AC), which can be kept for later use. Three unique characteristics to determine a photovoltaic cell's potency are ability to extract charge carriers to an external circuit, separate distinct types of charge carriers, and absorb light and excitation in bound and unbound electron-hole pair (Morris *et al.,* 2023). Research aimed at improving cell efficiency focuses mostly on the photoanode of a dye sensitized solar cell (DSSC) which is an example of concentrating photovoltaics (CPV) in the third generation where a variety of nanoparticles, hybrid composites, and doped films have been extensively employed (Prakash *et al.,* 2021). According to (Sharma *et al.,* 2015), the most widely used third-generation solar cells are concentrated dye-sensitized, polymer-based and nano crystal-based. DSSC is a type of solar cell that generates

electricity by mimicking the natural process of photosynthesis. It consists of transparent conducting electrode coated and sensitized with dye molecules that absorb sunlight. Electrons in the dye are excited and are injected into the conduction band where they move out to the external circuit, producing electric current (Lathouwers *et al.,* 2013). Studies to enhance the efficiency of dye sensitized solar cell are majorly on the photoanode as charge transfer and light harvesting happen at the photoanode. The wide band gap is used in enhancing its stability under illumination of the solar rays. The various ways in which one can improve the workability of a DSSC include: increasing the concentration of the dye, enhancing the dye loading and improving on light absorption by having a light scattering layer over the active layer(Kaliramna *et al.,* 2022) The layer having a high concentration of dye has its own setback, as interaction of dye molecules increases, a thick insulating layer is formed and gets deactivated. Semi conducting materials which are porous and have a high bandgap provide a good surface for dye loading without increasing its concentration. Figure 1.3 shows a dye sensitized solar cell (DSSC).

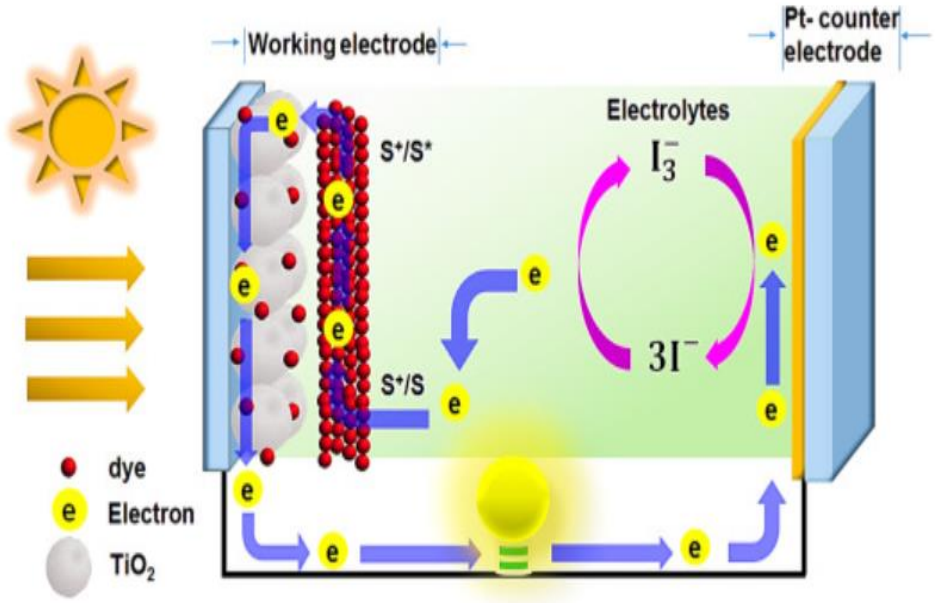


Figure 1.3: Diagram illustrating Dye sensitized solar cell(Kaliramna *et al.,* 2022)

Numerous transition metal oxides (TMO) have been deliberated for possible use as photoanodes, including tin oxide, cadmium selenide, titanium dioxide, zinc oxide (ZnO), and cadmium oxide (CdO) among others (Xaba *et al.,* 2017).Researchers have

recently shown a significant deal of interest in creating nanoscale semiconductor particles because of their size-dependent optical and electrical properties(Kiprotich *et al.,* 2022a). Due to their numerous technical uses and basic scientific significance, scientists have been paying close attention to the development of these nanoparticles (Bansal, 2019). Gas sensors, phototransistors, optoelectronic devices and photovoltaics are just a few of the many industrial and commercial applications that are driving up demand for high-quality, dependable photovoltaic devices (Ullah *et al.,* 2017). Metal oxides are good candidates due to their excellent properties in terms of electrical conductivity, structural and optical. The investigation of nanoparticles with varying sizes, compositions, and consistent morphological traits has garnered a lot of interest lately(Nasir *et al.,* 2013). Among transparent conducting oxides (TCOs) for solar cells, cadmium oxide (CdO) is one of the most promising examples employed initially in the early 1900s (Fall *et al.,* 2021). The crystal structure of cadmium oxide is a cubic phase, and a n-type semiconductor. Cadmium oxide is one of the metal oxide nanostructures that has garnered significant interest for a range of applications, including photodiodes and solar cells. This is due to its low electrical resistivity and good visual transmittance in the visible spectrum (Xaba *et al.,* 2017). One drawback of using cadmium oxide as the photoanode is its bandgap, which is 2.5 eV for a direct bandgap and 2.1 eV for an indirect bandgap (Sai & Marjorie, 2022).

Researchers are particularly interested in CdO because of its big energy band gap, high transmission constant in the visible spectrum domain, high luminescence and other aspects (Ullah *et al.,* 2017). Because of these properties, it can be used to create a variety of products, including transparent conducting oxides (TCO), diaphanous electrodes, phototransistors, photodiodes, infrared detectors, optoelectronics, and anti-reflection coatings (Kim *et al.,* 2007). The moderate electron mobility and higher carrier concentration of CdO, made possible by gullible contributions due to intrinsic stoichiometry, CdO exhibits high optical transparency and strong electrical conductivity in the solar spectrum's visible region (Jasim *et al.,* 2020).

Both the optical band gap and energy band gap of cadmium oxide nanoparticles can be varied through capping, doping and calcination during the synthesis. Capping is a process whereby the agent's surfactants stop particles from grouping together during colloidal reactions and help to manage the development of nanoparticles as stabilizers.

Adding dopants such as tin, fluorine, copper, zinc among others is known to stabilize the electrons in the metal oxide and adjust the crystal structure, conductivity, the place of energy bands, and make changes in the surface state (Mazhar *et al.,* 2023).

The study aimed at synthesizing and characterizing cadmium oxide nanoparticles and investigated effects of capping ratio on the optical and structural properties of cadmium oxide nanoparticles (NPs). It also investigated effects of tin (Sn) doping on optical and structural properties of NPs by varying the concentration of tin (Sn) and finally effects of adjusting the calcination temperature on structural, and optical properties. In the synthesis of tin (Sn) doped cadmium oxide (CdO) nanoparticles (NPs) for possible solar cell applications, this research employed precipitation by reflux method in making the nanoparticles. The technique is a simple wet chemical process which is effective and produces a highly crystalline nanoparticles of uniform surface with strong photoluminescence emission. Characterization of structural, and optical properties of nanoparticles was done using different analytical techniques. Fourier transform infrared spectroscopy (FTIR) was used to analyse molecular composition and functional groups present in the nanoparticles, X-Ray diffraction (XRD) was used to analyse the structural properties, UV-Visible spectroscopy (UV-Vis) was used to investigate their optical properties. The nanoparticles synthesized and characterized in the study possessed better structural and optical properties suitable for the development of solar cells with increased efficiency, environmentally friendly, economical and a renewable source of energy.

1.2 Statement of the problem

The reliance on fossil fuels poses a serious global concern, owing to their role in exacerbating climate change. Fossil fuel extraction and use have major environmental consequences, such as habitat destruction, water contamination, and air pollution. The burning of natural gases, oil and coal has led to global warming by releasing large amounts of carbon dioxide and other greenhouse gases into the atmosphere, contributing to global warming. The transition to renewable energy sources is important for reducing greenhouse gas emissions, mitigating the negative effects and fostering a more sustainable future. More affordable and efficient solar cells are required to help replace non-renewable energy. Solar cells have employed silicon-based technology extensively, although it is expensive. The third-generation dye-

sensitized solar cells (DSSC) are an alternative component to employ in tackling the problem of cost; however, they have low total power conversion efficiency. DSSCs used as the photoanode is less effective in conversion of light energy to electrical energy, therefore cadmium oxide is a semiconductor material which is better placed to be used as a photoanode in photovoltaic cells. The wide energy band gap of cadmium oxide is a setback which contributes to its low efficiency in conversion of light energy to electrical energy when used as a photoanode in photovoltaic cells. To reduce the energy band gap doping is done using transition element with smaller ionic radius like tin (Sn), copper (Cu), magnesium (Mg) etc. This enhances the compound's visual, electronic, and structural qualities by introducing electrons in to cadmium cations. The synthesis and characterization of cadmium oxide doped with tin (CdO: Sn) nanoparticles for potential application as a photoanode in solar cells form the basis of the study.

1.3 Objectives of the study

1.3.1 General objective

To synthesize and characterize tin doped cadmium oxide (CdO: Sn) nanoparticles for solar cell applications.

1.3.2 Specific objectives

1. To synthesize and characterize cadmium oxide nanoparticles using wet chemical process.
2. To investigate the effects of capping agent on the structural and optical properties of CdO nanoparticles.
3. To study the effects of tin (Sn) doping on the structural and optical properties of CdO nanoparticles.
4. To determine the effects of varying the calcination temperature on structural and optical properties of CdO: Sn nanoparticles

1.4 Research Questions

1. What is the effect of synthesizing cadmium oxide nanoparticles using wet chemical process?
2. How does the capping ratio affect the structural and optical properties of CdO nanoparticles?

3. Does the variation of tin doping level have effect on the structural and optical properties of CdO nanoparticles?
4. What are the effects of varying calcination temperature on the structural and optical properties of (CdO: Sn) nanoparticles?

1.5 Significance of the study

In the recent past, solar energy has drawn significant attention compared to traditional sources like fossil fuels which are exhaustible in nature and pollute environment since it is environmentally friendly and renewable source of energy. Nevertheless, its cost and effectiveness are a major setback and need to be addressed by synthesizing parts of a photovoltaic cell which is more effective and less costly. Synthesis and characterization of CdO: Sn nanoparticles for use as photoanodes in solar cell applications is crucial in the renewable energy area. Cadmium oxide is an n-type semiconductor with a wide energy bandgap and good optical transmittance in the visible region of spectra. Its properties can be fine-tuned to obtain good material suitable to be used as a photoanode in solar cell. In the global drive to battle change in climate change and reduce greenhouse gas emissions, the usage of renewable energy sources, such as solar energy, has grown in importance. Enhancing solar cell efficiency lowers the cost of producing solar energy and reduces the over-reliance on non-renewable resources like fossil fuels, which helps to reduce the consequences of climate change. By providing important insights into the structural, optical, and photoluminescence characteristics of CdO: Sn nanoparticles, this study may aid in the creation of more economical and efficient solar technology cells.

1.6 Scope of the study

This research focused on the synthesis and characterization of tin-doped cadmium oxide nanoparticles. It optimized the capping agent, dopant, and calcination temperature only. 3-Mercaptopropionic Acid ($C_3H_6O_2S$) and tin (Sn) were used as the capping agent and dopant material, respectively. A specific range of tin doping concentration was explored to understand the effects of doping. The reagents were used as obtained from the manufacturer without further purification.

1.7 Contribution of the study

i. Synthesis of Pure and doped CdO nanoparticles. The study carried out a successful combination of pure and Sn-doped CdO nanoparticles in a wet

chemical process. Each factor, such as the capping ratio (MPA), the doping concentration (Sn) and the calcination temperatures, has also been optimized to have CdO nanoparticles with fine-tuned structural and optical properties. The controlled method of synthesis has the potential to increase the output of the CdO nanoparticle that is applicable in a variety of optoelectronic applications.

ii. Optimization if the structural property. The face-centred cubic structure of CdO remained after Sn doping as verified by X-ray diffraction (XRD) analysis and there were no secondary phases. Crystalline size was found to increase with the temperature of calcination and reached the peak of 27.98 nm at 500^0C and the crystallinity of material would have been improvement. At an optimum calcination temperature of 350^0C, the distance between the crystallites, and the integrity of the crystallites, were found to be optimally harmonized thus reducing defects and strain in the solar cell's material, which is the key to solar cell efficiency.

iii. Enhanced Optical Properties, based on UV-Vis analysis, it was found the optical band gap of the CdO nanoparticles could be modified by ratios of capping and doping concentration. Sn doping reduced the bandgap to 1.812 eV which suited the nanoparticles better to light absorption in solar cells with a decreased bandgap of 5.5 eV. Such flexibility in band gap is crucial in enhancing the optics of the sunlight capture and improve their efficiency in converting solar energy.

1.8 Organization of the Thesis

The thesis has been arranged into five chapters, with chapter one having the background information of the study, statement of problem, objectives of the study, research questions, significance, scope and limitation of the study.

Chapter two discuss the literature information of the study that include, solar cells nanoparticles, methods of synthesizing nanoparticles and characterization techniques.

Chapter three outline the materials and reagents that were used in the synthesis process and procedure of obtaining the nanoparticles for the study. It outlines how each nanoparticle was obtained as per the objectives and the techniques that were used to characterized nanoparticles.

Chapter four discuss the results obtained from characterization of nanoparticles using XRD, UV-Vis, FT-IR, and PL The results are discussed as per the objectives order.

Chapter five highlights the summary and conclusions. It has been summarized based on the order of objectives. The recommendation from the study and recommendation for future work has been outlined.

CHAPTER TWO

LITERATURE REVIEW

2.1 Introduction

This chapter provides a comprehensive review of existing literature relevant to the synthesis and characterization of metal oxide nanoparticles, with a particular focus on cadmium oxide (CdO) and its tin-doped derivatives. It explores the fundamental properties of CdO nanoparticles, including their structural, optical, and electronic characteristics, and how these properties can be modified through doping. The chapter also reviews the role of tin (Sn) as a dopant, its influence on CdO properties, and the mechanisms by which doping enhances material performance in various applications such as optoelectronics and photovoltaics. Finally, discussion on the various synthesis methods for CdO nanoparticles, with emphasis on the wet chemical technique used in this study. A comparison of different synthesis approaches is made, highlighting their advantages and limitations.

2.2 Sources of Energy

Energy is the capacity of a system to do work and it takes forms, such as kinetic energy (energy of a body in motion), potential energy (energy stored in an object due to its position), and thermal energy (energy due to the motion of particles in a substance and the energy carried by electromagnetic waves(Bansal, 2019). As human populate, man has tried to harness more elements like wind, sun, water, geothermal, bio-mass and tidal to replace the depleted fossil fuels like natural gas, oil and coal and other biological materials(Bekele & Sintayehu, 2022). The use of energy is a major contributor to global climate change. Energy has further been classified as renewable or non-renewable sources. The renewable sources of energy include solar energy; energy obtained from the radiation of the sun and captured using a transducer (solar panel) which converts it to direct current electricity. Energy consumption has increased due to population growth in the world(Rathore *et al.,* 2021). Currently, old energy sources including gas, oil and coal, are used to meet the demand for energy (Bansal, 2019). Fossil fuel consumption increases greenhouse gas emissions and other pollutants that are bad for the environment and cause global warming. Because they are clean, renewable energy technologies have gained a lot of traction and have the ability to meet the world's energy needs (Langat *et al.,* 2022). Due to its low cost and

ease of installation, solar photovoltaic technology is employed in developing nations to electrify rural regions; nevertheless, a significant drawback is its low total energy conversion efficiency(Mohammad Bagher, 2015).

According to (Tala-Ighil,2015), the triple-junction combination InGaP/GaAs/InGaAs solar cell has the best conversion efficiency, at 37.9%. Solar cells are made by joining p-type and n-type materials close together, and they use this collector to divide the electron-hole pairs that arise from the sunlight hitting the solar cell. According to (Kamkird *et al*., 2012), following diffusion through the depletion zone, electrons reach p-type semiconductor and start producing a current when they gain heat energy. A light-induced current is higher if the material's carriers move more easily and/or if the p-n junction covers a bigger area (Lathouwers *et al*., 2013). All of these points to the need for cheaper and chargeable mobile semiconductor materials that can be produced in mass.

2.3 Classification of solar cells

In recent years, there has been a notable increase in the usage of solar cells, particularly photovoltaics, as a cleaner energy source. The evolution of solar cells can be divided into four generations: the first, second, third, and fourth.

2.3.1 First-generation solar cell

First-generation solar cells were developed using Silicon wafers. This technology's high-power efficiency makes it the oldest and most popular (Sharma *et al.,* 2015). The first-generation solar cells are further subdivided into two subgroups: monocrystalline silicon solar cells and multifocal silicon solar cells.

The monocrystalline solar cell is manufactured using the Czochralski technique (Bansal, 2019). Si crystals are carved from large ingots in this Czochralski method. The method of "recrystallizing" is more costly(Morris *et al.,* 2023). Since precise processing is necessary when producing the huge single crystal (Green *et al.,* 2022) The industry leader SunPower Corporation (2015) created modules with an efficiency of 20.4%, whereas monocrystalline silicon solar cells had an efficiency of 14% to 18%. (Mohammad Bagher, 2015).

The polycrystalline silicon solar cell is made up of several distinct crystals. This kind of solar cell is more cost-effective since it is processed by cooling a mold filled with graphite. At the moment, these solar cell types are the most widely used (Sharma *et al.,* 2015). Despite being cheap to produce, these cells have an efficiency of roughly 12–14%, which is comparable to monocrystalline silicon solar panels (Jasim *et al.,* 2020).

2.3.2 Second generation solar cells

Three main types of these thin-film photovoltaic technologies are amorphous (also called a-Si), micro morph, and silicon. Solar cells made in the second generation are cheaper than those produced from silicon wafers. Almost 350 nanometres of light-absorbing material is found in first-generation solar cells, but for thin-film solar cells it is 1 micrometre thick (Langat *et al*., 2022). Such thin-film polycrystalline silicon solar cells have power conversion efficiencies greater than 19%, thanks to both light trapping and back surface passivation. The solar cell's band gap is found to be 1.45 eV (Kamkird *et al*., 2012). This is made possible by the fact that a-Si solar cells need lower processing temperatures, allowing them to use cheap polymers and similar flexible materials. When fabricating, doped silicon chips are placed at the back of the silicon substrate. The surface facing sunlight is dark brown, and the other side is silver and the main problem with these cells is that their efficiency can change(Kaliramna *et al.,* 2022).

2.3.3 Third-generation solar cells

These involve technologies like concentrating photovoltaics (CPV) and organic photovoltaic cells that still require research and demonstration. According to (Sharma *et al.,* 2015), the most widely used third-generation solar cells are concentrated, dye-sensitized, polymer-based, and nano crystal-based. Third-generation technology improves the subpar electrical performance of second-generation technology while maintaining low production costs. (Kamkird *et al.,* 2012). One way to improve efficiency is to use the heat produced by UV radiation to increase voltage collection and incident spectrum concentration.(Rathore *et al.,* 2021).Modern researches target high conversion efficiency of 30-60% while maintaining cheap prices(Green e*t al.,* 2022). Increasing efficiency and lowering the price of solar cells per unit of power

generated are the two main methods utilized to lower the cost of photovoltaic electricity. Figure 2.1 shows different generations of solar cell technologies.

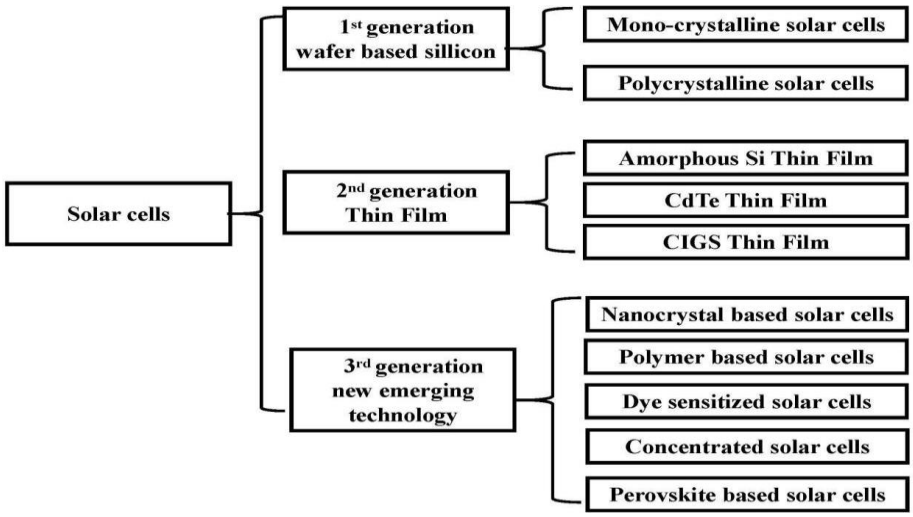


Figure 2.1: Generation of solar cell technologies (Lu, 2023)

The temperature, colour and intensity of the incident light affect the electrical output voltage(Lee *et al.,* 2007) This is evident from the data obtained by Ogherohwo *et al.,* 2015, for crystalline solar cell showing variation in the emission wavelength versus the conversion efficiency as shown in Table 2.1.

Table 2.1: Output power and conversion efficiencies of the crystalline solar cell.

(Ogherohwo *et al.,* 2015)

Colour	Wavelength Range (nm)	Current (A)	Voltage (V)	Power (W)	Efficiency (%)
Red	625-780	0.25	6.35	1.58	7.34
Orange	595-625	0.21	6.09	1.28	5.92
Yellow	575-595	0.22	6.15	1.35	6.25
Green	495-595	0.24	6.24	1.42	5.91
Blue	455-495	0.19	6.01	1.21	5.65

2.4 Properties of CdO

The optical bandgap of cadmium oxide differs by 1.94 eV between pure cadmium oxide and tin-doped nanoparticles produced by microwave irradiation (Prakash *et al*., 2021). The optical bandgap reduced as the tin doping concentration rose as follows: Sn (5%, 10%, and 15%) doped nanostructures with cadmium oxide had respective

optical bandgaps of 2.02 eV, 2.0 eV, and 1.69 eV. Cadmium oxide nanoparticle prepared by thermal-treatment with polyvinyl pyrrolidone (PVP) as the capping agent and calcined at 500 ^{0}C and above reports that the sample before calcination shows an amorphous behaviour but structurally appeared crystalline-like. And Calcined samples as observed in the XRD patterns display a sharper and narrower diffraction peak indicating crystal formation of the CdO nanoparticles *(*Al-Hada *et al*., 2017) The morphology of the cadmium oxide nanoparticle was uniform, and the particle size was relatively good at calcination temperatures of 500^0, 550^0, 600^0 and 650^0 measuring 23, 28, 37, and 41 nm, respectively. Further increase in calcination temperatures demonstrated an enhanced crystallinity of the particle by increasing the intensity peaks and eliminating the undesired small peaks that appeared at low temperatures(Morris *et al.,* 2023). Particles have a tendency to melt their surfaces and fuse together to form bigger shapes as the temperature rises.Transparent conductive oxides with good properties prepared by physical vapor deposition method at elevated temperatures reported that Indium doped cadmium oxide has high electron mobility resulting in high conductivity while minimizing free carrier absorption (Gary Kwok *et al.,* 2019) Synthesis of copper oxide nanoparticles using simple wet chemical method done and XRD patterns confirmed the formation of highly crystalline crystals and morphology of CuO NPs alongside XRD data are polycrystalline in nature (Samanta *et al.,* 2017) the synthesized NPs exhibited strong photoluminescence emission peaked at 485nm.

Synthesis of Indium doped cadmium oxide thin films by sol-gel process, reports a transparent conductive metal oxide even before sintering process and after sintering and annealing in the temperature range of 200-600 ^{0}C, the particle size increases as a result enhancing electrical properties(Gary Kwok *et al.,* 2019)increased indium doping concentration led to increase in resistivity of the cadmium oxide due to the degradation of the crystallinity and with further increase in doping >12%, resulted in total loss of crystallinity ,forming an amorphous cadmium oxide doped with indium 203 alloys. Semiconductors with energy band gap in the range of 1eV to 1.5eV, (827 nm to 1240 nm near infrared) has great potential to be used as a photoanode due to the efficiency needed in solar cell.

Cadmium oxide is a binary oxide classified as an n-type semiconductor with a direct energy band gap of 2.2 to 2.5 eV (Xaba *et al.,* 2017). It consists of a rock salt face

centred cubic structure (FCC; a=0.469nm) which is polycrystalline with alternating Cadmium and Oxygen atoms located at the lattice (Kathalingam *et al.,* 2018). The Figure 2.2 shows the cubic structure of cadmium oxide.

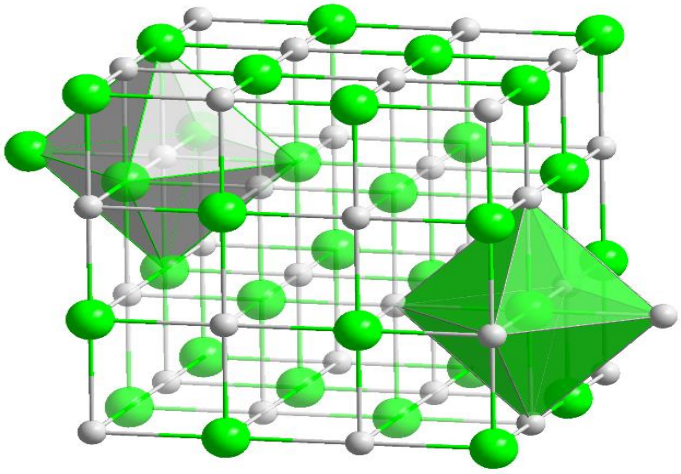


Figure 2.2: Crystal structure of cadmium oxide (Pan & Zhu, 2015)

Cadmium oxide possesses high capacity for absorption and emission of radiations a good material for solar cell applications among transparent conducting oxides. The high electrical conductivity and optical transmittance of CdO in the visible region of solar spectrum, shows great potential for use as the photo anode in solar cells. (Udoka *et al.,* 2020)

2.5 Effects of Capping Agent

The functions of a capping agent depend on having a polar head group and a nonpolar tail. The polar part of the molecule aligns with the metal, while the tail is in contact with the nearest surroundings (Javed *et al.,* 2020). By controlling the size and shape of solar cell applications, their ligands maintain the bond and organization of the nanoparticles with the environment where they are produced, supporting their appearance and optical qualities. For this reason, surfactants stop particles from grouping together during colloidal reactions and help manage the development of nanoparticles as stabilizers (Latha *et al.,* 2017).

2.6 Effects of Tin (Sn) Doping

Cadmium oxide among the transparent semiconductors has low optical band gap in comparison with the others. The optical band gap could be widen without altering the

electrical properties by doping with metallic impurities having ionic radius less than that of cadmium ions, could increase electrical conduction and optical properties(Udoka *et al.,* 2020). Tin is the most favoured dopant which substitute cadmium cations by controlling and enhancing optical and structural properties of CdO (Yusuf *et al.,* 2017). Since Sn^{4+} ions have four valence electrons ($5s^2$, $5p^2$) and ionic radius of 0.69 Å which is smaller than that of Cd^{2+} ions (0.95 Å), it is anticipated that increasing electron concentration will improve electrical conductivity. Additionally, since Sn^{2+} ions have ionic radii of 83 pm and Cd^{2+} ions have 109 pm, the optical band gap will shift in together with the increase in CdO transparency (Kathalingam *et al.,* 2018). A slight increase in Sn doping concentration increases the crystallite size of the nanoparticle and a further increase in doping causes re-orientation of the crystallites because a smaller amount of tin doping concentration allows the crystals to coalesce, hence increasing crystal size. Tin atoms affect CdO lattice by producing oxygen vacancies, tin substitutes, and stress variation, which increases the lattice parameter (Zhenguo Ji *et al.,* 2011).

2.7: Effects of Calcination Temperature

Calcination is a process that brings about thermal decomposition, phase transition, or removal of volatile materials when a substance is heated in the absence or presence of oxygen. A nanoparticle's crystallite size grows as the calcination temperature rises, and the surface areas that result are inversely correlated with the crystallite size (Morris *et al.,* 2023). Optical energy gap increases with an increase in the calcination temperature of the nanoparticle due to the increase in the crystallite size and decrease in defect states near the bands (Nasir *et al.,* 2013).

2.8: Method of Synthesizing Nanoparticles

Various methods such as sol-gel process, co-precipitation, physical vapor deposition, thermal treatment, microwave radiation and precipitation by reflux method, among others, have been employed in the synthesis of nanoparticles.

Precipitation method is a simple wet chemical process that is cost-effective in the preparation of nanoparticle and confirms the formation of a highly crystalline nanoparticle, uniform surface with strong photoluminescence emission along XRD results (Samanta *et al.,* 2017).

Figure 2.3 shows schematic diagram for the preparation of cadmium oxide nanoparticles.

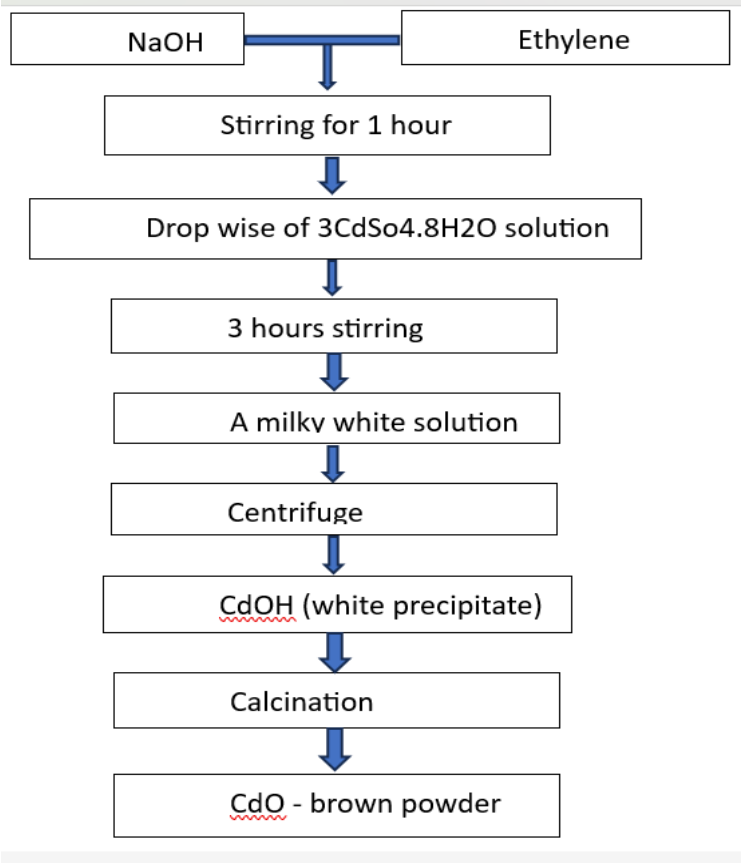


Figure 2.3: Preparation of cadmium oxide nanoparticles (Al-Hada *et al.*, 2015)

2.9: Chapter Summary

This chapter provides a comprehensive review of literature relevant to the research. It begins by highlighting the limitations of fossil fuels and their contribution to environmental challenges such as climate change and global warming. The discussion also outlines sources of energy and transitions into renewable energy, with a focus on solar cells and how nanotechnology is improving their performance. Special attention is given to cadmium oxide nanoparticles, discussing how capping, doping and calcination temperature influence their structural and optical properties. The chapter further explores wet chemical method of synthesis for the nanoparticles.

CHAPTER THREE

MATERIALS AND METHODS

3.1 Introduction

This chapter presents the detailed methodology adopted for the synthesis and characterization of tin-doped cadmium oxide (CdO: Sn) nanoparticles using the wet chemical method. The choice of this method is based on its simplicity, cost-effectiveness, and ability to produce nanoparticles with controlled morphology and composition. The chapter outlines the materials and reagents used, preparation techniques, doping procedures, and conditions under which the synthesis was carried out. Furthermore, it elaborates on the various characterization techniques employed to analyse the structural, optical, morphological, and elemental properties of the synthesized nanoparticles. Techniques such as X-ray diffraction (XRD), UV-Vis spectroscopy, Fourier-transform infrared spectroscopy (FTIR), photoluminescence (PL), and scanning electron microscopy (SEM) are discussed in relation to their role in understanding the properties and behaviour of the doped nanoparticles.

3.2 Materials

3.2.1 Reagents

The following reagents were used in the synthesis process purchased from Sigma Adrich and A.B.Chem.Co., Ltd. All chemical reagents were of analytical grade and were used without further purification

- Cadmium acetate di-hydrate Cd $(CH_3CO_2)_2$ with 98% purity.
- Mercaptopropionic acid $C_3H_6O_2S$ (MPA) 98%- capping agent
- Sodium hydroxide (NaOH)
- Ethanol 99.9% -Precipitating agent
- Deionized water -Solvent
- Tin chloride ($SnCl_2$) 98%

3.2.2 Apparatus

The following are some of the equipment used in the synthesis process.

- 100mL glass beakers
- Magnetic stirrer with a hot plate with a thermocouple

- PH Meter
- Muffle furnace
- Crucibles
- Weighing balance
- Pestle and mortar
- Three necked flasks

3.3 Methods

3.3.1 Synthesis of CdO Nanoparticles

The procedure for synthesis of CdO NPs was borrowed from(Al-Hada *et al.,* 2015) with a few modifications as follows: 1 mmol cadmium acetate dehydrate was dissolved in 100 mL of deionized water to form a clear solution. This was followed by dropwise addition of 50 mL 1M NaOH solution under vigorous stirring until a white precipitate of cadmium hydroxide ($Cd(OH)_2$) was formed. The pH of the solution formed was adjusted to pH 10 using a pH meter. The mixture was transferred to a round-bottom three-necked flask and refluxed under continuous stirring for 2 hours at 80 °C. The solution was removed from the hotplate and allowed to cool to room temperature. The CdO NPs were rinsed several times using deionized water and ethanol in the centrifuge at 2000 rpm. The CdO NPs were dried in an oven at 100 °C before annealing at 350 °C in the muffle furnace for 2 hrs. The CdO NPs were kept in sample holders for further analysis.

3.3.2 Capping of CdO nanoparticles with Mercaptopropionic Acid (MPA)

According to (Wageh, 2014), the procedure was modified, and the steps are as follows: 2 ml of MPA was added to the pre-synthesized CdO nanoparticle dispersion. Using a magnetic stirrer, the mixture was stirred continuously to ensure that the MPA interacts with the surface of the CdO nanoparticles. The solution mixture was heated to 80 °C and maintained under reflux for 2 hours. The heated solution was removed from the hotplate and allowed to cool to room temperature. The CdO NPs was rinsed several times using deionized water and ethanol in the centrifuge at 2000 rpm. The MPA-capped CdO NPs were dried in an oven at 100 °C before annealing at 350 °C in the muffle furnace for 2 hrs. The MPA-capped CdO NPs were then kept in sample holders for further analysis. This procedure was repeated for different capping ratios (0.5ml, 1ml, 1.5ml, 2.5ml, 3.0ml and 3.5ml).

3.3.3 Tin Doping of MPA-Capped CdO Nanoparticles

To synthesize Tin doped MPA capped CdO NPs, the procedure from (Prakash *et al.,* 2021) was used with few modifications as follows; 1 mmol cadmium acetate dehydrate was dissolved in 100 mL of deionized water to form a clear solution. This was followed by dropwise addition of 50 ml 1M NaOH solution under vigorous stirring until a white precipitate of cadmium hydroxide ($Cd(OH)_2$) was formed. Then, 2 mL of MPA was added to the pre-synthesized CdO nanoparticle dispersion. Using a magnetic stirrer, the mixture was stirred continuously to ensure that the MPA interacts with the surface of the CdO nanoparticles. In a separate beaker tin chloride ($SnCl_2$) was dissolved in 10ml deionized water to obtain portions of 0.5%, 1%, 1.5%, 2.0%, 2.5%, 3.0%, and 3.5% mol to Cd. The tin precursor solution was added slowly to the CdO dispersion while stirring continuously to ensure uniform doping. The pH of the solution formed was adjusted to 10. The mixture was then transferred to a round-bottom three-necked flask and refluxed under continuous stirring for 2 hours at 80 °C to allow tin atoms to integrate into the CdO lattice. The refluxed solution was removed from the hotplate and allowed to cool to room temperature. The CdO NPs was washed several times using deionized water and ethanol in the centrifuge at 2000 rpm. The CdO NPs was then dried in an oven at 100 °C before annealing at 350 °C in the muffle furnace for 2 hrs. The MPA- capped CdO: Sn NPs were kept in sample holders for further analysis. To study the effects of Sn doping concentration on the CdO NPs, the procedure was repeated for 1%, 2.0%, 2.5%,3.0% and 3.5% tin concentrations.

3.3.4 Calcination Process

The as-prepared MPA-capped CdO: Sn NPs were divided into ten (10) portions. Each portion of the MPA-capped CdO: Sn NPs was placed in ceramic crucibles. To study the effects of different calcination temperatures on the material properties of the MPA-capped CdO: Sn NPs, the samples were heated in a muffle furnace at different calcination temperatures (Morris et al., 2023), ranging from 200 ^{0}C to 650 ^{0}C at step of 50 ^{0}C for 2 hrs. Calcined samples were kept in sample holders for further analysis. Figure 3.1 shows steps of synthesizing MPA capped CdO nanoparticles doped with tin (Sn) through precipitation method.

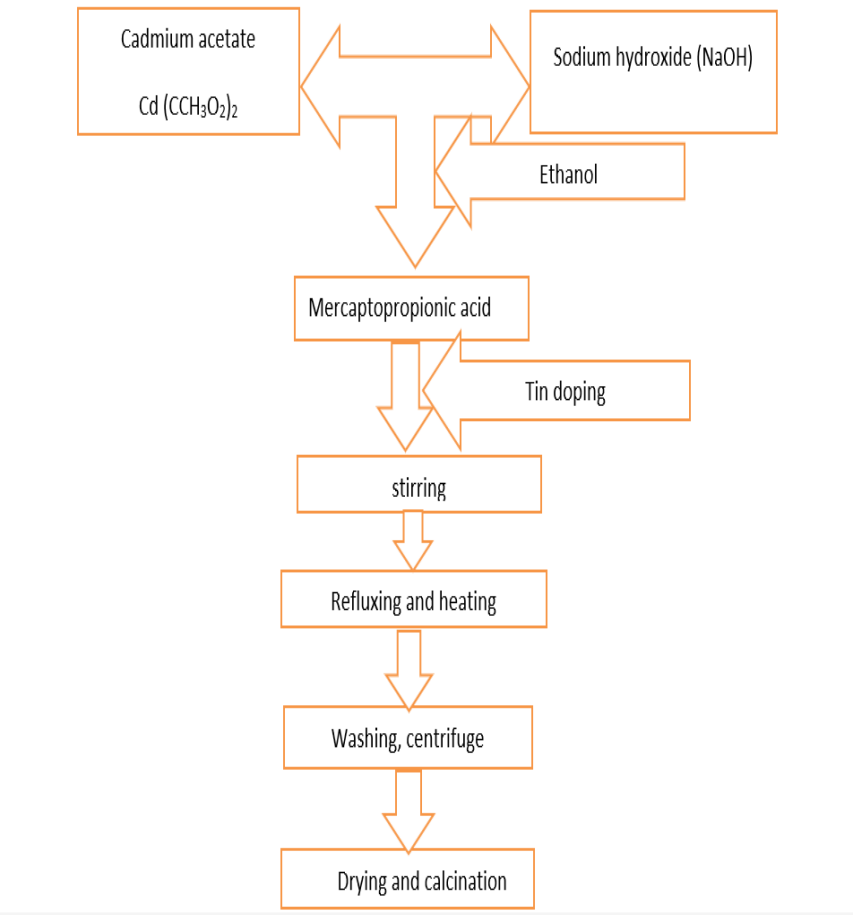


Figure 3.1: Preparation of MPA capped cadmium oxide nanoparticles doped with tin through precipitation by reflux method.

3.4 Analytical Techniques

3.4.1 X-Ray diffraction (XRD)

A non-destructive analytical method for figuring out a material's crystalline structure is X-ray diffraction (XRD). It is made up of an X-ray tube that emits an X-ray beam, a sample chamber that holds the sample, and a detector that logs the pattern of X-rays that the sample diffracts. The sample's crystal structure determines the precise angles at which the atoms in the sample will diffract the X-rays when the X-ray beam interacts with them. The detector records the pattern of diffracted X-rays, and the resulting data are analysed to determine the crystal structure of the sample(Bunaciu *et al.,* 2015). Applications for the data gathered by XRD equipment are numerous and include materials science, geology, chemistry, and biology. It offers a quick and non-destructive method of figuring out a sample's crystal structure without destroying it. X ray diffractometer is shown in Figure 3.2.



Figure 3.2: ARL EQUINOX X-ray diffractometer at Murang'a University of Technology.

The sample was ground to pieces and made uniform so that all the particles were small and fine, and then put into a sample holder. Beams of X-rays were aimed at the sample and the pattern recorded was checked to determine its crystal size, lattice parameters, and full width at half maximum. To find the lattice spacing of nanoparticles, Bragg's equation was used as $n\lambda = 2dsin\theta$ with λ being the wavelength, θ the angle of incidence, and d the interplanar spacing. To calculate their average crystal size, Scherrer equations were used: $L = \frac{K\lambda}{\beta cos\theta}$ where λ stands for wavelength, β presents the full width at half maximum, and K is a constant. From the equation below, the distance a between (100) planes is found, and c is the distance between (002) planes; $a = \frac{\lambda}{sin\theta\sqrt{3}}$ (Bunaciu *et al.,* 2015).

3.4.2 Fourier transform infrared spectroscopy (FTIR)

It works on the premise that some infrared IR radiation is absorbed by a sample as it passes through, and the remaining radiation is then recorded. Because FTIR is faster than other analytic tools, it is far more sensitive and precise, and it does not harm the sample being analyzed; it is chosen over other methods. In the pharmaceutical sector,

petrochemical engineering, food analysis, and the identification of components in a mixture, analytical techniques are employed to identify organic, polymeric, and inorganic materials. The Fourier transform and increased speed are made possible by the interferometer, which serves as the infrared source in FTIR. A mathematical function called the Fourier transform breaks down waves and yields the wave's frequency as a function of time. An interferogram is a graph that is produced by the interferometer. The interferogram is transformed into the infrared spectroscopy spectrum graph that we utilize via the Fourier transform. On a graph, the spectrum is displayed with the transmittance on the y-axis and the wave number on the x-axis. FTIR provides a wealth of information about the chemical composition of a sample including chemical identification where the chemical functional groups present in a sample are identified. The unknown sample spectrum is compared to with the known spectra in the library. It is also used in quantitative analysis in determining the concentration of a specific chemical compound in a sample by measuring the intensity of its absorbance band. In structural analysis the position and shape of the absorption bands in FTIR can provide information about the molecular structure of a compound. The process includes preparing the sample, which can be done as a pellet or a thin film. The second phase, sample measurement, entails passing infrared radiation through a sample holder while the sample is within. The sample's absorption or transmission of radiation is measured. The sample is next subjected to spectral analysis, in which the FTIR machine uses a Fourier transform algorithm to turn the time-domain signal into a frequency-domain spectrum. The resulting spectrum is then examined to determine the sample's chemical makeup (Mohamed *et al.,* 2017). FTIR is used in environmental monitoring to check for pollutants in soil, water, and air samples; material characterization to examine the molecular structure of materials like polymers, ceramics, and composites; forensic analysis to track down evidence like fibers, paints, and medications; and pharmaceutical analysis to guarantee the quality and purity of medications. Figure 3.3 shows FTIR spectrometer.

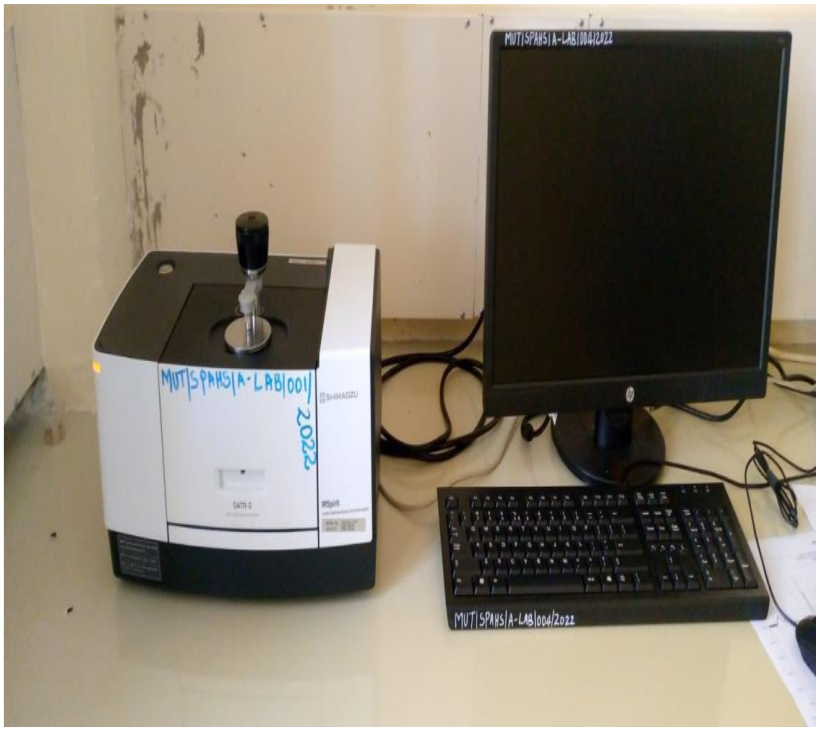


Figure 3.3: Shimadzu IR Spirit FT-IR model at Murang'a University of Technology

The samples were made into pellets and fine powders, then put inside a sample holder. The infrared radiation moves through the sample, and it measures how much radiation is absorbed or sent through. Spectral analysis concludes the process as the FTIR machine takes the given signal and transforms it into a spectrum to identify what the sample is made of (Mohamed *et al.,* 2017).

3.4.3 Ultra-Violet visible spectrometer (UV-Vis)

UV-vis spectroscopy is a technique that works by having Ultraviolent (UV) or visible (Vis) shine light on a sample and measure the amount absorbed by the sample at various wavelengths. It gives us information about the composition and chemical structure of the sample. There exist two operation routes which are the absorbance mode and transmittance mode. In the absorbance mode, the amount of light absorbed by the sample is measured as a function of wavelength, and a graph of absorbance vs wavelength is obtained, this graph is known as absorption spectrum and is used to identify the presence of specific chemical groups in a sample. In the transmittance mode, the amount of light transmitted through the sample is measured as a function of wavelength. A graph of transmittance vs wavelength known as a transmission

spectrum is used in determining the concentration of a particular compound existing within the sample. UV obeys the Beer-Lambert law which is given by A= Log (Io/I) = ECL (Picollo *et al.,* 2019) where A is absorbance, Io represents light intensity incident upon the sample, I represent the intensity of light that leaves the sample. C shows the molar concentration of the solute. L and E represent the length and molar absorptivity respectively. This technique is employed in quantitative analysis to determine the concentration of a specific compound in a sample, in qualitative analysis to determine the presence of chemical groups, in kinetics studies to monitor chemical reactions in real time, and in environmental and pharmaceutical analysis(L.C. Passos & M.F.S. Saraiva, 2019). Figure 3.4 outlines the scanning electron microscopy.



Figure 3.4: Evolution one plus UV-Vis spectroscopy at Murang'a University of Technology

The samples were dissolved in deionized water and then placed inside the cuvette. The spectroscopy was powered on and adjusted with the help of a standard reference material. Following this, only wavelengths within the range of 200-800 nm were selected for the experiment, and background scanning took place to find out the absorbance and transmittance of the sample. Using Tauc's equation, we found out the band gap of the nanoparticles (Baishya *et al.,* 2018) $\alpha h\nu = A(h\nu - E_g)^n$ with A is a fixed parameter, and hv measures the photon energy, Eg is the band gap, and n is 2 for indirect allowed transition or ½ for direct transition. The relationship between the band

gap energy (Eg) of semiconductors and (ahv) is tied to the energy of a photon (hv) (Picollo *et al.,* 2019).

3.4.4 Photoluminescence Spectroscopy (PL)

PL spectroscopy involves the excitation of electrons in a material and the subsequent emission of light as electrons return to their ground state. This technique is essential for studying the electronic structure and defect states in nanoparticles. In semiconductor nanoparticles like quantum dots, PL analysis can reveal information about bandgap energies, surface defects, and quantum confinement effects. For instance, the photoluminescence behaviour of metallic nanoparticles, such as gold nanoflowers, has been studied to understand their emission properties, which are influenced by factors like shape and size samples were loaded to microscope which was operated under vacuum to ensure high quality imaging. The spectroscopy was used to determine the surface morphology and size distribution of nanoparticles. Figure 3.5 shows SP-LF97 model PL spectroscopy at Murang'a University of Technology



Figure 3.5: SP-LF97 model PL Spectroscopy at Murang'a University of Technology

3.5 Chapter Summary

This chapter comprehensively discusses the materials used, the synthesis method followed in achieving the specific objectives of the study, and the characterization techniques employed to analyze data. The method used in the study is precipitation by

the reflux method, and characterization techniques employed include FTIR, XRD, UV-Vis, and PL.

CHAPTER FOUR

RESULTS AND DISCUSSION

4.1 Introduction

This chapter delves deeply results and discussions under the structural, elemental composition, chemical- functional bonding and optical properties of MPA capped cadmium oxide doped with tin nanoparticles synthesized using wet chemical process. As part of the first specific objective of this research, synthesis of cadmium oxide (CdO) nanoparticles was accomplished through the utilization of the wet chemical precipitation technique on a reflux basis. This method was chosen because it is easy, cheap, and can be used in generating uniform nanoparticles. The reaction also resulted in the formation of CdO precipitates with resultant increased colour mixing as well as consistency upon reaction and drying process due to nucleation and nanoparticle growth. The result of the synthesis was also modified by the further characterization methods, including XRD, FTIR, and UV-Vis spectroscopy, which confirmed the creation of CdO with the expected crystalline and optical properties. This preliminary synthesis process allowed research into the results of doping, capping, and calcination described below.

4.2. Investigating the effects of capping ratio on the structural and optical properties of Mercaptopropionic acid-capped cadmium oxide nanoparticles.

4.2.1 X-ray Diffraction (XRD) Analysis

The XRD patterns of MPA-capped CdO nanoparticles prepared with different concentrations of the capping agent are shown in Figure 4.1. The major diffraction peaks (111), (200), (220), and (311) observed in the figure are indexed to the cubic structure of CdO as evidenced from JCPDS No.01-073-6494. The nanoparticles had a preferential growth orientation along plane (200) and (220) with an increased peak intensity at 2ml MPA capping. This is attributed to the enhanced crystallinity of the nanoparticles. The XRD peaks of CdO were sharp in the case of 2 mL MPA capping compared to other levels of the capping agent, which indicates good crystallinity of the nanoparticles. The XRD patterns of MPA-capped and uncapped CdO nanoparticles prepared with different concentrations of MPA are shown in Figure 4.1.

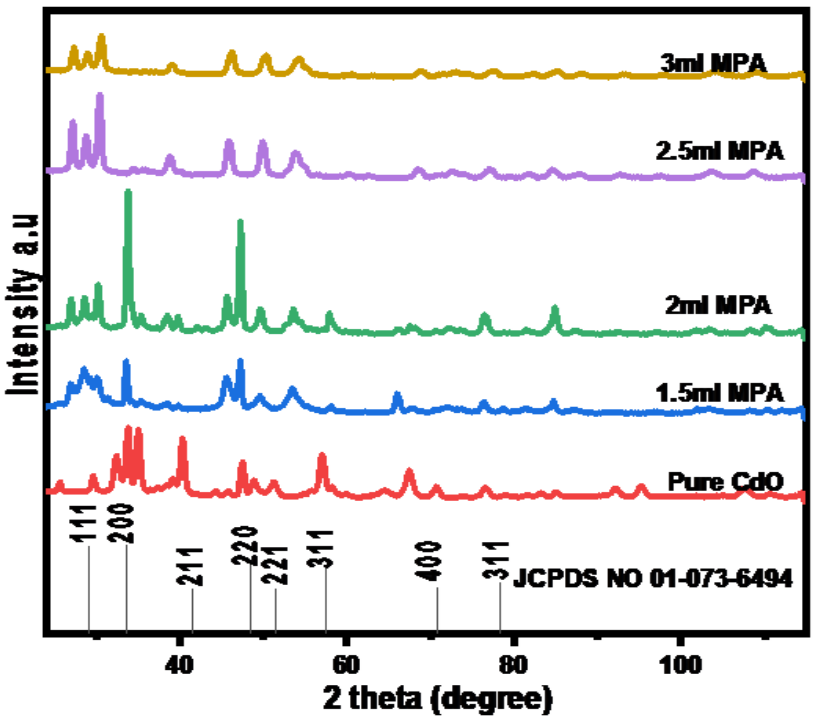


Figure 4.1: The XRD patterns of MPA-capped and uncapped CdO nanoparticles prepared with different concentrations of MPA.

The crystallite was calculated using the Debye–Scherrer equation; the size of the crystallites depended strongly on the capping ratio. Pure CdO contained spherical crystals with an average size of 21.38 nm as shown in Table 4.1. The crystallite size rose to 26.10 nm upon the addition of 1.5 ml MPA and to 24.17 nm after 2.0 ml MPA was used. At first, stabilization provided by MPA molecules helped control the first nucleation with little effect on further crystal growth. Even so, increasing the capping ratio to above 2.5 ml and 3.0 ml decreases the crystallite size, and the values reach 17.80 nm and 15.20 nm, respectively. This reduction is attributed to the high surface passivation from extensive use of the MPA, which reduces movement of atoms and stops more grain growth (Albin *et al.,* 2021). According to (Wiengnon & Anuragudom, 2019), MPA helped reduce the size of CdSe nanoparticles by blocking aggregation and coalescence. In another study, (Rahdar, 2013) also observed the exact effect in thiol-based ZnS particles, attributing it to the close-packed arrangement of the thiol ligands around the nanoparticle surfaces. Small changes in the lattice parameters and d-spacings in Table 4.2 were noticed with different capping ratios. When CdO was capped with 2.5 ml MPA, the amount of expansion in the unit cell was visible in the increased lattice parameter of 0.508 nm, compared to 0.459 nm for

pure CdO. This can be attributed to the strain caused by the binding of the surface MPA groups, such as carboxylates and thiols, interacting with Cd^{2+} ions and disrupting the local atoms around them. The same shifting of XRD peaks and unit cell parameters due to MPA capping was observed by in CdS and CdSe quantum dot assemblies (Nelson *et al.,* 2016). It was also revealed that both lattice strain and the number of dislocations depended greatly on the amount of capping. With 1.5 ml and 2.0 ml of MPA added, the strain went down from 0.0056 in pure CdO to 0.0046 and 0.0049. For dislocation density, it also dropped to a minimum at 1.5 ml MPA (0.00147 nm^{-2}) and then increased again as the MPA levels rose (to 0.00433 nm^{-2} at 3.0 ml MPA). Table 4.1 shows the crystallite sizes of MPA capped CdO nanoparticles and Table 4.2 outlines the average d spacing, lattice parameters, strain and dislocation density of CdO nanoparticles.

Table 4.1: Showing the crystallite sizes of MPA-capped CdO NPs

Mercaptopropionic acid (MPA) capping ratio (mL)	**2θ**	**FWHM β**	**Intensity**	**Crystallite Size D (nm)**
Pure CdO	33.793	0.38831	1262.5	21.38
1.5	33.599	0.31790	936.02	26.10
2	33.805	0.34347	2822.9	24.17
2.5	30.433	0.46255	1679.5	17.79
3	30.614	0.54192	733.73	15.19

Table 4.2: Showing average d spacing, lattice parameters, strain and dislocation density of MPA capped CdO NPs

Mercaptopropionic acid (MPA) capping ratio	**d-Spacing**	**Lattice parameter**	**Strain**	**Dislocation Density**
Pure CdO	0.2650	0.4590	0.0055	0.0021
1.5 ml	0.2665	0.4616	0.0045	0.0014
2 ml	0.2649	0.4588	0.0049	0.0017
2.5 ml	0.2934	0.5083	0.0074	0.0031
3 ml	0.2917	0.5053	0.0086	0.0043

Balancing the ligands, leads to better ordering of the crystals, though it can alter the structure at higher levels. In a study by (De León-Gutiérrez *et al.,* 2006), it was

observed that having more CdO or surfactants in the film increased lattice strain and made crystals less orderly. A photovoltaic perspective suggests that larger crystallites and fewer lattice disorders enhance charge carrier transfer in solar panels and stop charges from reforming. According to these findings, applying MPA capping ratio of 1.5–2.0 ml gives the best balance between encouraging crystal growth and covering the surface with a protective layer. As the materials are capped at higher levels, the effects of quantum confinement could get better; however, more defects and stress within the material might affect how well they function in solar cell applications. In this way, adjusting the capping concentration plays an important role in designing MPA capped CdO nanoparticles for optoelectronics and photovoltaics.

4.2.2 UV-Vis

UV–Visible absorption spectroscopy was applied to find out how different amounts of MPA covering each CdO nanoparticle influence how they absorb and reflect light. It is essential to use the optical absorption edge and band gap to assess how suitable nanomaterials are for solar cell photoanodes. Figure 4.2 shows the absorbance spectra.

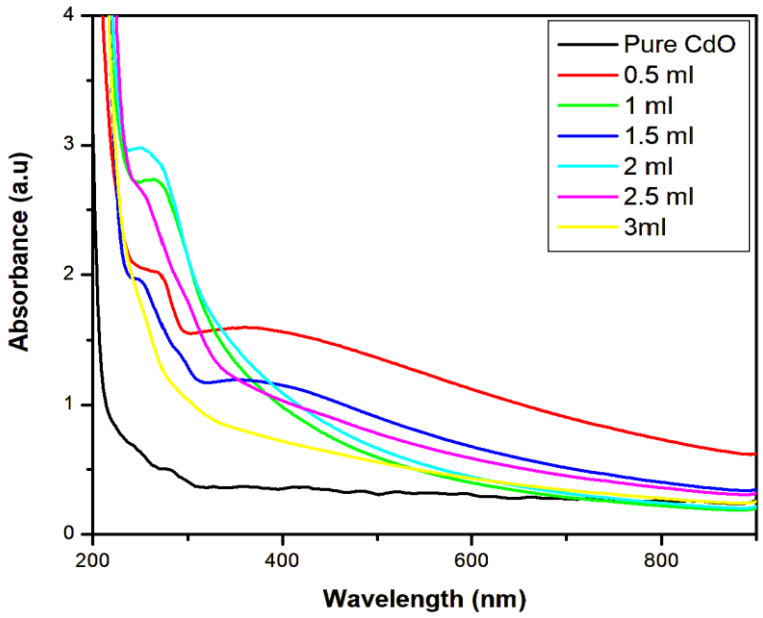


Figure 4.2: The evolution of absorbance spectra of CdO nanoparticles for different concentrations of the capping agent.

The UV absorption band seen in both pure and capped nanoparticle spectra is a sign of wide-band-gap semiconductors. Most importantly, the capped samples have

stronger absorption at both the UV and part of the visible portions of the spectrum than pure CdO. Micro-structured particles alter the way they scatter and absorb light because of changes in their surface activity and particle size caused by the MPA molecules. When the rate of MPA ratios was increased, the position of the absorption edge shifted a lot. At first, when the ratios went from 0.5 to 1.5 ml, the absorption edge shifted to a lower energy range, showing the band gap became smaller. However, when the MPA was increased further (2.5–3.0 ml), there was a slight shift, reversing into the blue which is usually connected to smaller molecules and effects from quantum confinement. Both attachment of ligands and the way crystallites are arranged on the surface appear to be key in how the transitions in the material take place. Related findings were reported by (Pattabi, 2003), as they observed that moderate capping increased visible light absorption, yet too much capping resulted in less absorption because there was less aggregation and more electron restrictions in the NPs.

4.2.3 Bandgap analysis

The estimation of the band gap in pure CdO and Sn-CdO nanoparticles was done using Tauc relation formula (4.1).

$$(\alpha hv)^{\gamma} = Ahv - AE_g \qquad 4.1$$

Here, absorption coefficient is denoted by α, the incident photon energy by hv, the allowed transition by γ, constant by A, and electronic band gap of the semiconductor material by Eg. When γ equals 2 there is indirect transition and when it equals ½ there is direct transition from the valence band to transition region. Tauc's plot was used to draw a line from (αhv)2 that intercepted the x-axis where $(\alpha hv)^2 = 0$ to obtain the approximate energy band gap. Figure 4.3 shows the Tauc plot for the MPA capped cadmium oxide.

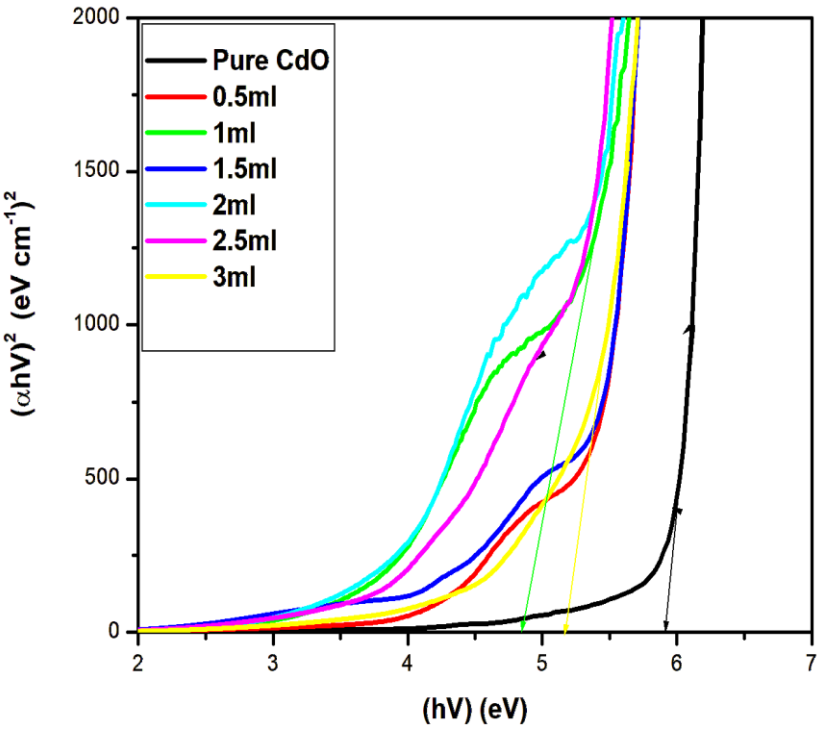


Figure 4.3: Tauc's plot for capped cadmium oxide nanoparticles with different concentrations of mercaptopropionic acid (MPA).

It is observed that the band gap of pure CdO is 5.5 eV, but it decreases to as little as 3.5 eV at 2.0 ml MPA capping before widening slightly. At low-to-moderate capping ratios, particles become more uniform, the strain in the crystal structure is less, and electrons are better shared, which causes the band gap to decrease. According to the Burstein–Moss effect, elevated carrier numbers may cause the band gap to appear broader, but the real gap is in fact narrower because the light needed for absorption is now moved to lower energies (Ivchenko, 2024). Since the narrowing is more noticeable at higher capping ratios, it is possible that too many particles are trapped by the shell, so they do not grow much and end up having bigger band gaps. Scientific research has shown that this happens in nanoparticles of capped semiconductors such as CdS and ZnS (Li & Li, 2006). The best photoanode materials should be able to absorb sunlight and must have a band gap between 1.8 and 3.5 eV for visible light harvesting (Mohd Raub et al., 2024). While 2.0 ml MPA result in a still relatively large band gap (3.5 eV), the change shows a major improvement compared to uncapped CdO. Because more light is absorbed and the gap narrows more here, the dye could work well in solar cells designed for higher efficiency. They agree with (Nelson *et al.,* 2016), who showed better optical properties in surfactant-modified CdO films planned

for solar energy uses. In addition, adjusting the proportions of CdO to other elements allows for efficient tuning of the nanomaterials for these uses. When samples are capped with 1.5–2.0 ml MPA, their absorption is good, and their energy bands are well aligned.

Notably, the observed band gap of pure CdO nanoparticles (5.5 eV) is considerably higher than the typical value of the band gap of bulk CdO (2.5 eV). This is attributed to the quantum confinement effect that manifests itself at the nanoscale (Jiang *et al.,* 2018). At this scale, materials experience distorted electronic structure stemming from the confined motions of the charge carriers in the nanoparticle. As a result, their optical and electronic properties, hence their band gap may differ significantly compared to their bulk values. Hence, the fact that the band gap of this study increases aligns with the behaviour that CdO showed when synthesized at the nanoscale. The obtained band gap values of MPA capped CdO nanoparticles were recorded in the Table 4.3

Table 4.3: Band gap values of MPA-capped CdO NPs

Mercaptopropionic acid (MPA) capping ratio (mL)	**Band gap (eV)**
Pure CdO	5.5
0.5	5.0
1	4.74
1.5	4.45
2	3.5
2.5	4.0
3	4.26

4.2.4 Photoluminescence

Photoluminescence spectroscopy was used to examine what happens to the defects and to the light-emitting properties of CdO nanoparticles when mercaptopropionic acid (MPA) is added as a capping agent. Since the emission of PL comes from recombining electrons and holes, examining the placement and intensity of PL bands gives insights into whether the material is of high quality and has any defects. Figure 4.4 shows the PL spectra of MPA-capped CdO.

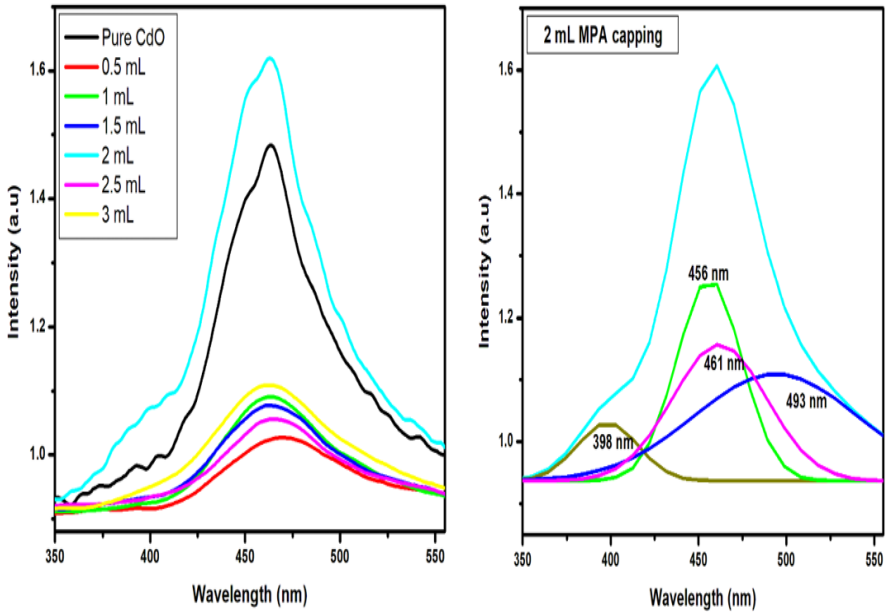


Figure 4.4: (Left) PL spectra of MPA capped CdO NPs and (Right) Gaussian deconvolution of 2.0 ml MPA capped CdO NPs.

All samples, pure and MPA-capped CdO nanoparticles, were found to emit blue light with their maximum emission at wavelengths of 460 nm and 470 nm. The spectrum showed that CdO emits PL at 463.83 nm, and this emission is very intense (0.145 a.u) as shown in Table 4.4. After capping, it was found that both the strength and color changes of the emission suggest that the electronic states of the material are impacted by being on the surface. The PL intensity (0.183 a. u) for the sample held with 2 ml MPA was highest, and the emission was shifted slightly towards blue at 461.83 nm. Because of more effective surface passivation by MPA molecules, there is less non-radiative recombination, which enables more efficient radiative transitions (Abid *et al.,* 2021). When the spectrum was deconvolved, it showed four clear peaks at 398, 456, 461, and 493 nm, which were due to band-edge and defect emissions. At 398 nm, the emission is mainly from excitonic recombination occurring at the bottom of the conduction band. In comparison, the emissions between 456–493 nm are connected to vacancies, Cadmium (Cd) impurities within the material, and defects from its surface, typical for CdO NPs (Contreras-Rascon *et al.,* 2020). When the capping volume was increased, the PL intensity performed differently from linear results. The reaction's strength dropped from pure CdO to 0.5 ml capping, shot up at 2.0 ml, decreased once again at 2.5 ml and 3.0 ml, and then stabilized. The observed behavior hints that at low MPA levels, passivation of defects is not strong enough, which causes a high level

of non-radiative recombination. 2 mL capping is most effective at passivating surface traps so that there is more radiative recombination. Further increases in the capping agent may affect the material's surface or stop crystals from developing quickly, which would reduce emission intensity (Shen *et al.,* 2023). It was observed that when the thiol concentration on CdSe and CdS particles was low to moderate, their fluorescence intensity was increased, but too much ligand caused it to decrease (Zhang *et al.,* 2009). This trend is similar to the findings from the crystallite size and strain measurement in XRD. The results indicated that a 2 ml solution of MPA had average crystallites (about 24 nm) and few lattice defects, aiding effective recombination of carriers. Strain and disorder became more common at higher capping ratios, and this is related to PL quenching. Higher concentrations of ligands make quantum confinement and carrier localization effects appear more clearly in nanosized crystals. Such effects have been observed in CdSe and ZnS nanocrystals, and changes in PL peak are explained by shifts in surface energy as well as alterations in their electronic states (Sukanya & Sagayaraj, 2015). Table 4.4 outlines emission wavelengths and relative intensities of MPA capped CdO.

Table 4.4: Emission wavelengths and relative intensities of MPA capped CdO NPs

Mercaptopropionic Acid capping ratio (mL)	**Emission Wavelength (nm)**	**Relative Intensity (a.u)**
Pure CdO	463.83	0.14549
0.5	472.67	0.08972
1	462.61	0.13466
1.5	460.08	0.12716
2	461.83	0.18296
2.5	465.43	0.12721
3	463.42	0.09670

4.2.5 FTIR Analysis

Fourier-transform IR spectroscopy was used to identify the structure of the CdO nanoparticles and their successful modification by MPA in different concentrations. CdO bands and organic layers were both visible in the spectra recorded at 400–

4000 cm^{-1}. Figure 4.5 shows the FTIR spectra for different levels of MPA capped CdO nanoparticles.

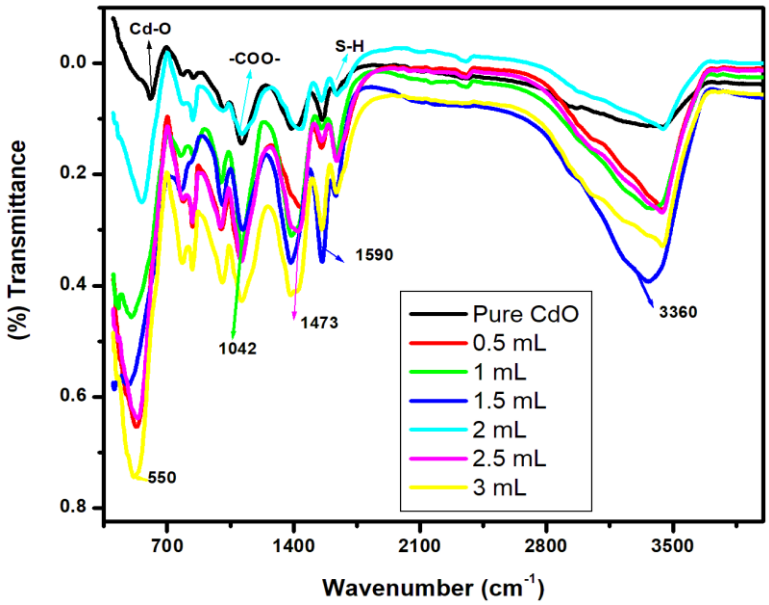


Figure 4.5: FTIR spectra of MPA-capped CdO NPs at different capping ratios.

In all the samples, an extensive absorption in the 490–600 cm^{-1} area was found, related to the Cd–O bond stretching. This confirms that cadmium oxide is present as the major product (Azzaoui *et al.,* 2023). Though strong across all energy levels, this band sharpens a lot more when MPA is added, showing that the oxide structure is becoming much more organized. A peak between 1000–1250 cm^{-1} was noticed in every sample with an MPA capping, which is related to vibrations of C–O groups and deformations of $-COO^-$ groups in the capping agent. It shows that the MPA molecule forms direct bonds with the CdO. When the capping ratio is increased, the formation of more intense peaks indicates stronger and wider surface coordination by MPA molecules. Furthermore, the region of the spectrum at 1460–1650 cm^{-1} is associated with S–H (thiol) stretching vibrations. Even the weak SH signals are found in capped samples, proving that surface Cd^{2+} atoms connect with the thiol groups via Cd–S bonds. This interaction helps to protect and manage the growth of particles while synthesizing them. A wide group of absorption bands around 3300–3500 cm^{-1} in pure and capped samples is assigned to the stretching vibrations of adsorbed moisture or surface hydroxyls. It is clear that the band intensity increases significantly in the capped

samples, especially when MPA concentrations go up, which can be attributed to the stronger attraction of the polar –COOH groups in MPA (Mandal *et al.*, 2023).

When the MPA concentration increases from 0.5 ml to 3.0 ml, the FTIR spectra demonstrate that the intensity of the carboxylate-related peaks rises and the peaks also shift slightly, which is evidence of greater surface functionalization. The stronger bands from COO- and the appearance of new S–H and C–H vibrations imply that MPA co-ordinates simultaneously using both its –COOH and –SH groups (Ellerbrock & Gerke, 2021). Once the capping is at its maximum (3 mL), the FTIR shows that the COOH groups have bound to the surface in well-defined, narrow peaks, suggesting perfect anchoring without many surface issues. On the other hand, when the sample volume is raised to more than 2.5–3.0 ml, the intricacy in vibrational patterns that appears could suggest that ligands in the system are crowding together, the surface is more loaded, or the system tends to aggregate (Yang *et al.,* 2025).From FTIR observations, it is clear that MPA can connect with CdO nanoparticles and also has a strong effect on their structure and surface chemistry. The vibrational modes identified reveal that MPA functional groups are present, which adds to the evidence from UV–Vis and PL measurements about changes on the surface. Using MPA leads to the passivation of traps, lowers the quenching of PL light, helps manage the growth of particles, and modifies the optical band gap. As shown by (Sukanya & Sagayaraj, 2015), the studies revealed that MPA capping of CdS and CdSe nanoparticles led to the appearance of new carboxylate and thiol bands in FTIR measurements and also made the nanoparticles more stable and improved their optical properties.

4.3 Effects of Tin doping concentration on the structural and optical properties of Cadmium oxide nanoparticles

4.3.1 XRD analysis

This investigation was done by making use of an X-ray diffractometer. For this reason, one can visually compare the as-prepared samples' crystal structures using XRD results with the information found in standard files. The XRD pattern for pure CdO as well as for tin doped CdO: Sn nanoparticles (made with 10ml tin chloride (0.5%, 1%, 1.3%, 1.5%, 2.0%, 2.5%, 3.0%, and 3.5% mol to Cd) solutions) was obtained using origin. A sample spectrum was taken by measuring XRD at angles (2Θ) from 0 to 120 degrees. The pattern seen in XRD at the peaks fits with JCPD card (073-6494), proving

that the sample's structure is a face-centred cubic polycrystalline one. XRD data for the peaks was indexed to (111) (200), (220), (221), (311), and (400) with the help of the XRD card file. The shapes of the peaks turned broader, and the tin-doped nanoparticles grew more often on (111) and (220) planes because of a higher doping level. The fact that the peaks at the higher doping levels are higher might show the improved crystallinity of the CdO nanoparticles. Because of the larger share of tin ions at 3.0% and 3.5% concentration, the lattice of CdO is no longer the same and this change is confirmed by XRD peaks. On Figure 4.6, you can see the XRD pattern for pure CdO as well as for doped CdO nanoparticles prepared with different amounts of tin and Figure 4.7 shows the XRD pattern for the major intense peak at (111) plane for doped and undoped CdO: Sn NPs synthesized through a wet chemical process.

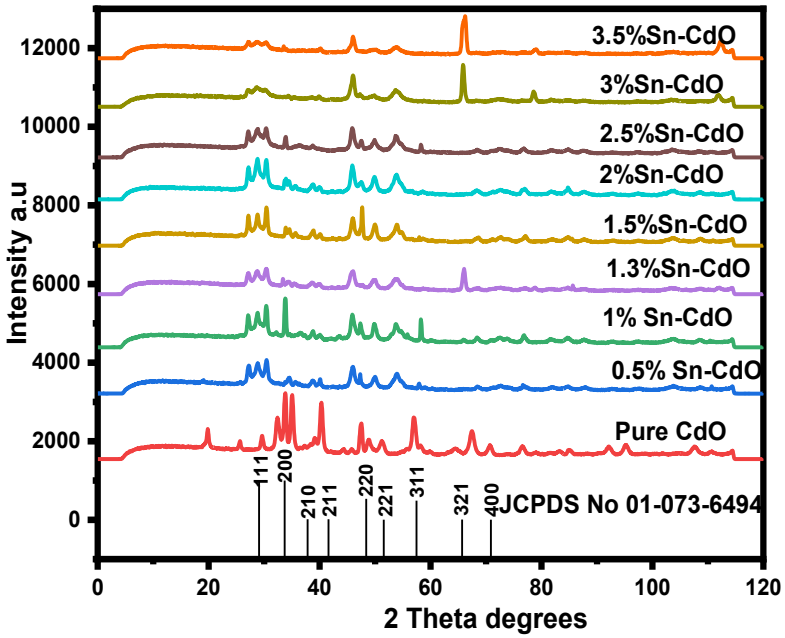


Figure 4.6: XRD spectra for the pure CdO and doped CdO with various concentration of tin prepared using wet chemical technique.

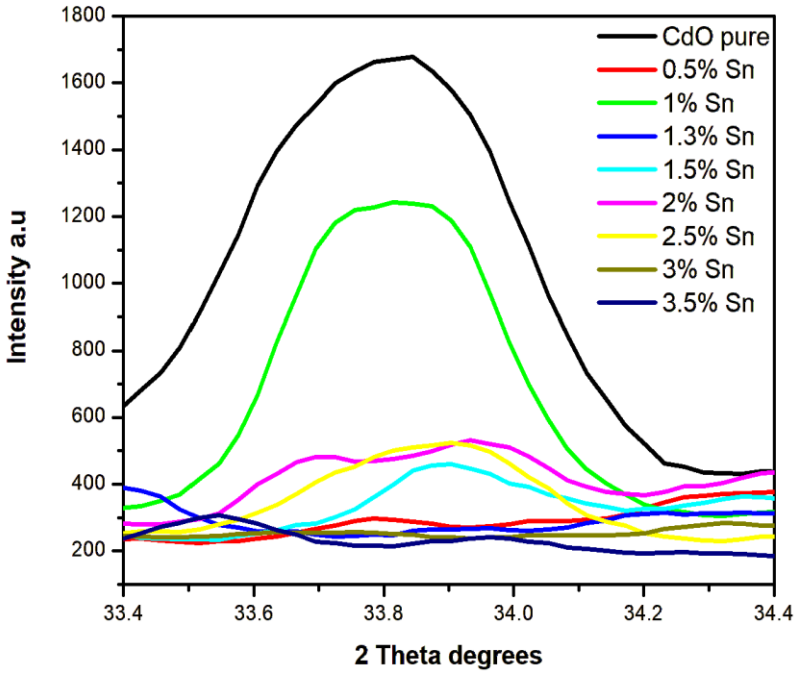


Figure 4.7: The XRD major intensity peaks for varying levels of tin for (111) plane synthesized using wet chemical process.

Debye Scherrer equation (4.2) was used to calculate the crystal size of nanoparticles (Al-Hada *et al.,* 2015).

$$D=\frac{K\lambda}{\beta_{hkl}Cos\theta} \qquad (4.2)$$

Where D is the crystal size, K is the constant equals 0.9, the wavelength of the radiation denoted by λ is 1.54960Å for copper Kα radiation, full width at half maximum (β_{hkl}) and θ is the peak position. A slight increase of Sn doping concentration (1%Sn) increases crystallite size of the nanoparticle from 20.07nm for pure CdO to 25.35nm tin doped, for 2.5%Sn the crystallite size increased to 24.45nm and further increase in doping (3.0%Sn) causes reduction of the crystallite size to 19.04nm. This could be attributed by a smaller amount of tin doping concentration allowing the crystals to coalesce hence enhancing crystallinity. Table 4.5 presents calculated crystallite sizes for plane (111) for pure and doped CdO.

Table 4.5: Tabulated crystallite sizes D (nm) using plane (111) for pure CdO and Sn-doped CdO

Concentration of Sn used to dope CdO (%)	2Ɵ	FWHM	β	Peak intensity	Crystallite size D(nm)
0	33.79	0.3957	0.006907	1651.99	20.07
0.5	33.80	0.1282	0.002237	297.19	61.98
1.0	33.81	0.3134	0.005470	1235.34	25.35
1.3	33.41	0.1491	0.002601	386.28	53.31
1.5	33.91	0.1666	0.002908	453.55	47.68
2.0	33.95	0.1204	0.002101	520.77	65.99
2.5	33.95	0.3249	0.005671	518.55	24.45
3.0	33.70	0.4167	0.007272	247.77	19.07
3.5	33.95	0.22168	0.003869	239.81	35.83

The lattice constant d was calculated using the Bragg's equation(4.3) (Fall *et al*., 2021)

$$n\lambda = 2d_{hkl}sin\theta \quad (4.3)$$

For Cadmium oxide face centred cubic structure, a=b=c therefore equation (4.4) was used to calculate lattice constant a

$$a = d_{hlk}\sqrt{h^2 + k^2 + l^2} \quad (4.4)$$

The calculated values of lattice constant a, and d spacing presented in the table 4.6 shows that the lattice parameters deviate slightly from the standard values. According to JCPD file no 00-005- 0640, plane (111) records d spacing of 0.2712nm. The deviation is attributed to by the tin doped cadmium oxide trying to adopt the lattice constant for pure cadmium oxide during the reaction. Also, the presence of strain in the nanoparticles could contribute to the lattice parameters deviation from the standard values. The micro strain (ε) values of the CdO:Sn were estimated using equation (4.5) (Kiprotich *et al.,* 2022b).

$$\varepsilon = \frac{\beta}{4\tan\theta} \quad (4.5)$$

Where θ is the diffraction angle and β is the full width at half maximum. The length of the dislocation lines per unit volume that is dislocation density (δ) was calculated by means of Williamson and Smallman equation (4.6) (Sidor, 2024)

$$\delta = \frac{1}{D^2} \quad (4.6)$$

Where D is the crystallite size obtained from the XRD results. Table 4.6 displays structural parameters for pure CdO and Sn doped CdO NPs prepared using wet chemical process. Generally, increase in the doping concentration the strain and dislocation decreased.

Table 4.6: Structural parameters for pure CdO and Sn-doped CdO

Concentration of Sn used to dope CdO. (%)	**d-spacing (nm)**	**Lattice parameter, a (Å)**	**Strain,$\mathcal{E}$**	**Dislocation density, σ**
0	0.2650	4.589	0.3257	0.00248
0.5	0.2649	4.588	0.1055	0.00026
1.0	0.2649	4.588	0.2578	0.00156
1.5	0.2641	4.458	0.1366	0.00044
2.0	0.2638	4.569	0.0985	0.00023
2.5	0.2638	4.569	0.2661	0.00167
3.0	0.2657	4.602	0.3439	0.00275
3.5	0.2638	4.569	0.1814	0.00078

4.3.2 UV-Vis analysis

The UV-Vis absorption spectrum was used to investigate the changes in optical properties of pure CdO and doped CdO NPs. Mostly, Ultraviolet-visible (UV-vis) spectrometer is used to measure bandgap energy (Eg) of semi-conductor materials dispersed in deionized with known coefficient. Aqueous solutions of the samples' nano powders were made using a liquid with an absorption coefficient that is known. Light absorption by the nanoparticles occurred at different points on the spectrum because of the doping concentration. The absorption edge of pure CdO is 298nm, but when a dopant is used, it increased and was between 300nm and 340nm. A dopant changes the electronic features of nanoparticles because of stress, strain, and types of

defects called interstitial and vacancies. The absorption wavelength of CdO is smaller than the normal wavelength since the quantum confinement effect appears once the CdO nanoparticles form (Bett *et al.,* 2024). Thanks to quantization, the band gap energy goes up, letting the materials absorb only wavelengths that are farther away from short wavelengths. In Figure 4.8, the UV-vis absorption spectra for pure CdO and CdO: Sn are shown.

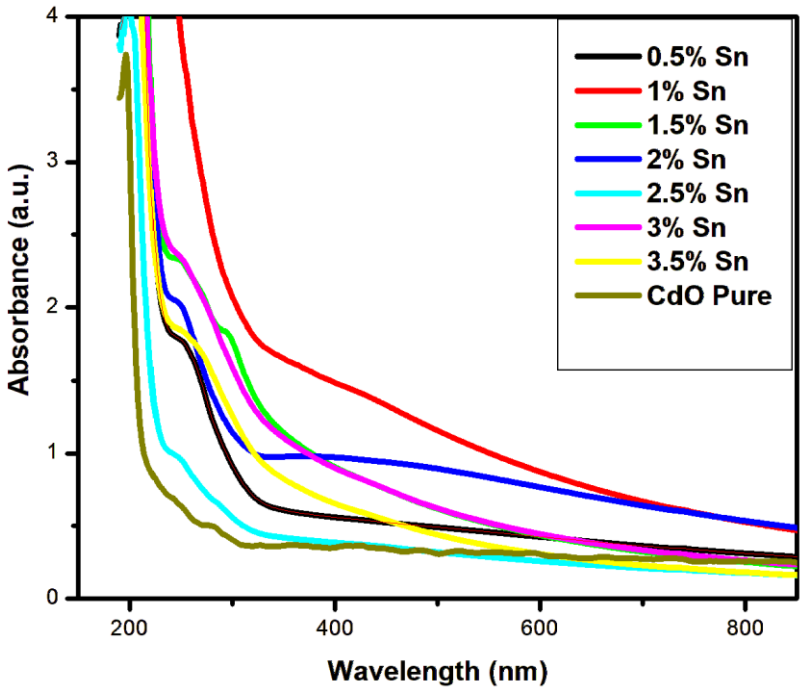


Figure 4.8: The evolution of absorbance spectra of different tin doping concentrations.

4.3.3 Band gap analysis

The organization of electrons in a material is guided by how large its band gap energy is. Tauc relation equation (4.7) (Othman, 2022) was used to predict the energy band gap of the as-obtained CdO and CdO:Sn NPs.

$$(\alpha hv)^{\gamma} = Ahv - AE_g \qquad (4.7)$$

Given α is the absorption coefficient, hv stands for the incoming photon energy, γ is the allowed transition in the semiconductor material, A is a constant, and Eg describes the electronic band gap of the semiconductor material. When γ was varied to 2, the allowed transition is indirect, while when it is ½ the transition is direct from the

valence band to the transition level. The tangent of $(\alpha hv)^2$ was drawn on Tauc's plot, and then extrapolated to the $(\alpha hv)2 = 0$ axis to estimate the band gap energies for different concentrations of doping. The Tauc's plot and the band gap energies for different concentrations of doping are displayed in Figures 4.9 (a) and (b) respectively.

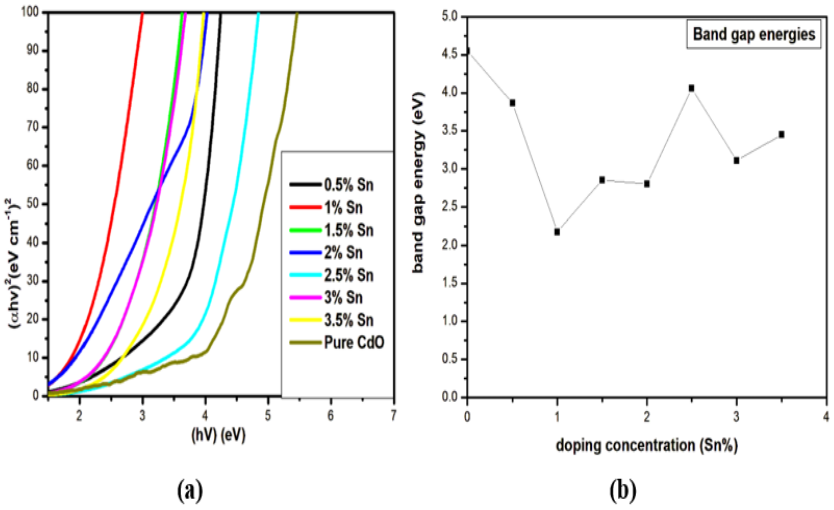


Figure 4.9: Tauc's plot (a) and band gap energies of the NPs (b) for different Sn doping concentrations.

From the Tauc's plot the band gap energy for pure CdO NPs was 3.68 eV and for doped CdO NPs ranges from 1.81eV to 3.52eV depending on the dopant concentration. It is found that as the doping concentration of tin increases, the bandgap energies decrease. The bandgap energies for doped and undoped CdO nanoparticles differ from the standard values of the corresponding bulk material. The discrepancies could be attributed to the lattice strain and dislocations during the formation of the nanoparticles. Table 4.7 presents the summary of the bandgap energies (eV), absorption edge (nm) and the corresponding concentration of tin.

Table 4.7: Summarized table showing absorption edge and bandgap energies for different concentrations of tin doping

Concentration of Sn used to dope CdO (%)	Absorption edge (nm)	Band gap energy (eV)
0	298	4.548
0.5	305	3.869
1.0	311	2.175
1.5	315	2.853
2.0	320	2.800
2.5	295	4.060
3.0	328	3.110
3.5	337	3.450

The increase in the UV region (298nm -337nm) with increasing tin doping concentration and reduction in band gap energy is attributed to enhanced electronic transitions due to modification of the band structure(Aadim *et al.,* 2020). When Sn^{4+} ions are incorporated into CdO lattice, they substitute Cd^{2+} ions and introduce extra free electrons into the conduction band due to charge compensation.(Kathalingam *et al.,* 2018) The increase in free carrier concentration leads to formation of defect states or shallow donor levels near conduction band from 4.548 eV to 2.175 eV.

4.3.4 Photoluminescence (PL) analysis

The photoluminescence properties of doped and undoped CdO nanoparticles were carried out at an ambient temperature and at an excitation wavelength of 320 nm, the photoluminescence properties of CdO were found to depend on the concentration of the dopant. Pure CdO was found to exhibit high luminance with an emission wavelength of 395nm compared to tin doped cadmium oxide which shows emission at wavelength in the range of 396nm to 400nm. Figure 4.10 shows photoluminescence emission spectra for CdO: Sn (a) and pure CdO (b) whereas Figure 4.11 shows the deconvoluted graph of 1.5% Sn doped.

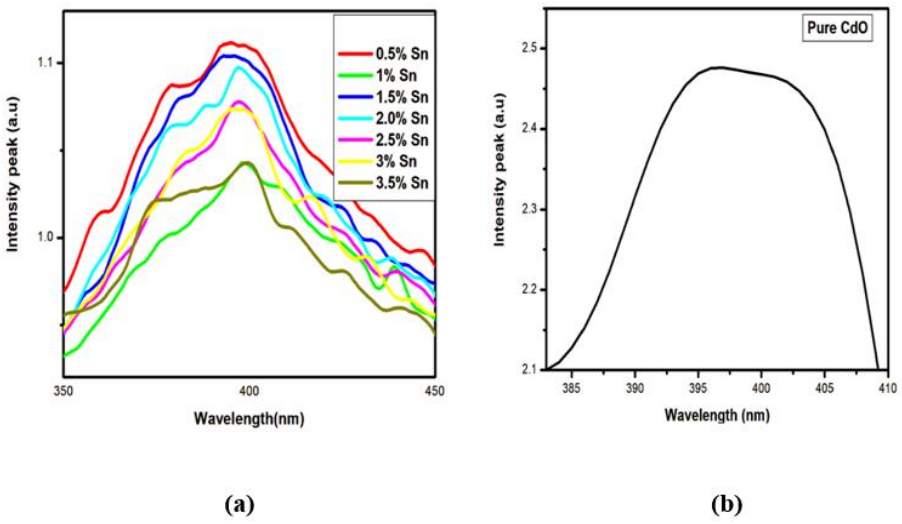


Figure 4.10: (a) Photoluminescence emission spectra of tin doped CdO and (b) undoped CdO.

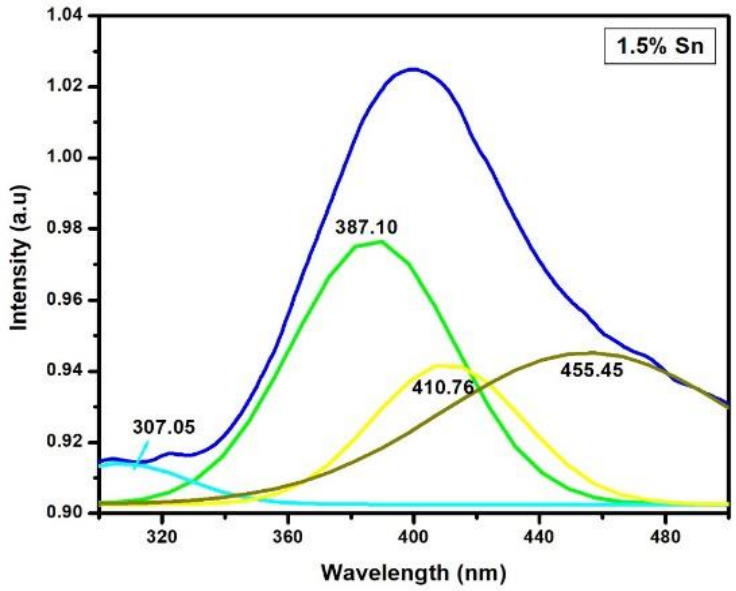


Figure 4.11: Deconvoluted graph of 1.5% Sn doping

The intensity of emission peaks was found to decrease with increase in doping concentration. However, at a higher concentration of tin doping, photoluminescence quenching was observed. This could be due to surface recombination caused by Sn ions which creates surface states that act as traps for photogenerated electrons and holes, preventing them from participating in emission of light (Gary Kwok *et al.,*

2019)This is also associated with the fact that highly doped nanoparticles excite electrons which can return to ground state without emitting photons. Table 4.8 shows a summary of tin doping concentration, emission wavelength and relative intensity for pure and doped CdO.

Table 4.8: Summary of tin doping concentration, emission wavelength and relative intensity for pure and doped CdO

Concentration of Sn used in doping CdO (%)	Wavelength (nm)	Relative intensity (a.u.)
0	395	2.470
0.5	398	1.11
1.0	399	1.04
1.5	393	1.10
2.0	396	1.09
2.5	397	1.07
3.0	397	1.07
3.5	400	1.04

4.4 Effects of varying calcination temperature on the structural, and optical properties of tin-doped cadmium oxide nanoparticles.

4.4.1 XRD Results

In this study, XRD was used to analyze the structure of both pure and tin Sn: CdO NPs synthesized via precipitation by reflux technique. Figure 4.12 shows the XRD pattern of all synthesized samples, and it corresponds well with the standard cubic phase of CdO (JCPDS No. 01-073-6494). This suggests the formation of desired material without any detectable secondary phases. The absence of impurity confirms successful incorporation of Sn ions into the crystal lattice of CdO, hence maintaining phase purity across varying calcination temperatures.

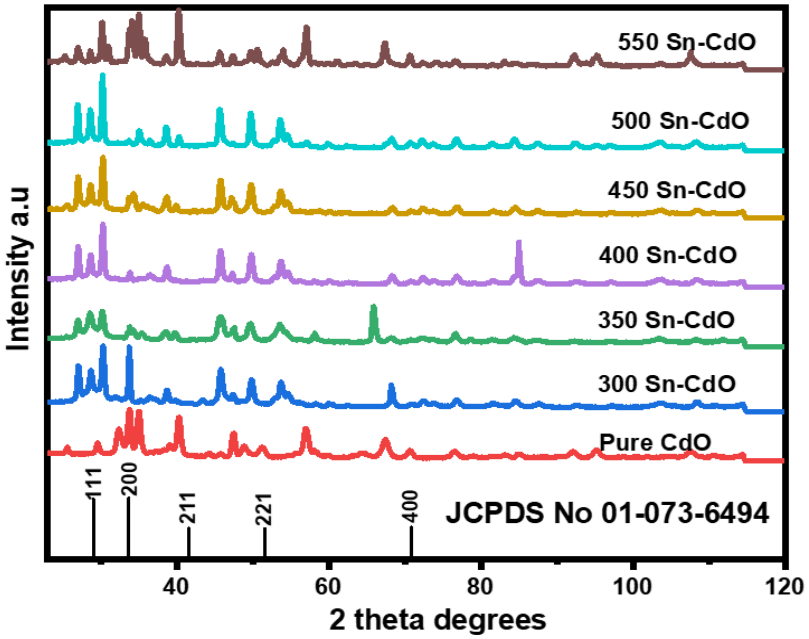


Figure 4.12: XRD pattern of synthesized Sn: CdO NPs at varying calcination temperatures.

The Debye-Scherrer equation was used to calculate the crystallite size of the nanoparticles, using the FWHM of their most intense diffraction peak. The results indicate a non-linear relationship between calcination temperature and crystallite size. The crystallite size increased from 21.22 nm in pure CdO to a maximum of 27.98 nm at 500°C when Sn was added. After that, there was a slight decrease to 26.25 nm at 550°C. At 350°C, the crystallite size was observed to decrease considerably, reaching 15.54 nm as shown in Table 4.9. This trend shows that calcination temperature influences crystallite growth. At lower calcination temperatures, there was limited thermal energy, which hindered grain growth, leading to smaller crystallite sizes (Zhao *et al.,* 2022). The sharp decrease at 350°C was attributed to lattice strain and defect deformation due to Sn doping, which impeded crystal growth (Zhao *et al.,* 2022). Increasing the temperature to 500°C leads to more atom mobility, inducing grain coarsening and secondary recrystallization, hence further reducing the crystallite size. The results are consistent with previous research. According to (Abbas *et al.,* 2021), higher calcination temperature results in better crystallinity and larger particles for CdO nanoparticles, attributing this to improved grain growth and reduced lattice imperfections. Moreover, (Karim *et al.*, 2025) reported that the crystallite size and crystallinity improved when CdO NPs were doped with silver and cobalt and treated

by heat, showing the significance of dopants and thermal treatment in shaping the structure. As the calcination temperature was increased from 300 °C to 500 °C, the crystallite size increased slightly from 23.71 nm to 27.98 nm, while the FWHM decreased, suggesting better crystallinity and reduced broadening of peaks due to fewer lattice imperfections. However, at a temperature of 350 °C, the crystallite size decreased significantly to 15.54 nm while the FWHM increased to 0.529^0, indicating that the material was strained or had not fully crystallized at this intermediate temperature. The findings consistent with (Abbas *et al.*, 2021) who stated that higher calcination temperatures leads to improved grain growth and reduced peak broadening due to atomic diffusion and availability of thermal energy. Likewise, research conducted by (Karim *et al.,* 2025) concluded that lower FWHM values were associated with larger crystallite sizes in silver and cobalt co-doped CdO NPs, highlighting the significance of the right thermal treatment to control structural properties.

Table 4.9: Showing the crystallite sizes of Sn: CdO NPs at varying calcination temperatures.

Calcination temperature (^{0}C) of Sn: CdO	**2θ (Degrees)**	**FWHM (Degrees)**	**Peak Intensity**	**Crystallite size D (nm)**
Pure CdO	33.793	0.39110	1267.3	21.22
300	30.336	0.34704	1530.1	23.71
350	30.251	0.52951	761.02	15.54
400	30.346	0.31543	1645.1	26.09
450	30.345	0.34573	1601.5	23.80
500	30.302	0.29410	2108.4	27.98
550	30.222	0.31343	1205.2	26.25

Both lattice strain and dislocation density play an important role in determining the physical strength and electronic features of semiconductors(Kiprotich *et al.,* 2022a). In this study, the Williamson-Hall technique was used to calculate lattice strain (ε), and the dislocation density (δ) was calculated from the crystallite size. Lattice strain equation (4.8), and dislocation density equation (4.9) were utilized in obtaining strain and dislocation density.

$$\varepsilon = \frac{\beta}{4 \tan \theta} \quad (4.8)$$

Here, ε represents the micro strain, θ is the diffraction angle of the most intense peak (200) and represents the FWHM in radians.

$$\delta = \frac{1}{D^2} \quad (4.9)$$

Where δ is the dislocation density in nm^{-2}, and D is the crystallite size (nm)

The results in Table 4.10 demonstrated that at 350°C, the strained material (0.0085) and the highest density of dislocations (0.0041 nm^{-2}) were observed, indicating the smallest crystallite size. Therefore, lower calcination temperature may result in more lattice defects and the creation of extra dislocations due to insufficient thermal energy (Seetawan *et al.,* 2011). At 500°C, the strain and dislocation density in the crystal became 0.0047 and 0.0012 nm^{-2} indicating less crystal strain and fewer defects. These findings align with previous reports; for example, (Bhosale *et al.,* 2021) discovered that calcining at higher temperatures minimized lattice strain and dislocation density of NPs, which they attributed this behavior to better crystallinity and defect healing in the material. Using a similar approach, (Dasuki *et al.,* 2023) noted that doping NPs nanoparticles with chromium (Cr) resulted to less strain and fewer dislocations. When calcined at higher temperatures, it demonstrated the impact of doping, thermal treatment, and structural defects in the nanoparticles.

The lattice parameter 'a' and interplanar spacing 'd' were obtained from the XRD data to understand how Sn doping and calcination temperature influence the crystal structure of CdO. The spacing between the atoms in the crystal increased from 4.590 Å in pure CdO to about 5.117 Å in samples where Sn was added at 550°C. The expansion is attributed to Sn^{4+} ions (ionic radius 0.83 Å) substituting the existing Cd^{2+} ions (ionic radius 0.95 Å), making the cubic unit cell bigger (Ikram *et al.,* 2021). The values of d-spacing showed a similar pattern, rising higher with an increase in calcination temperature and Sn doping. This shows that higher calcination temperatures facilitate the incorporation of Sn into the CdO lattice, leading to equal lattice expansion (Anitha *et al.,* 2019). Adjusting these structures is key to changing the electronic and optical properties of CdO nanoparticles for photovoltaic devices.

Table 4.10 outlines the calculated lattice parameters, d spacing, strain, and dislocation density of synthesized CdO: Sn NPs using wet chemical process at varying calcination temperature.

Table 4.10: Tabulated lattice parameters, d spacing, strain, and dislocation of synthesized Sn: CdO NPs at varying calcination temperatures

Calcination temperature (^{0}C) of Sn: CdO	d-spacing (nm)	Lattice parameter, a (Å)	Strain ε	Dislocation density δ (nm^{-2})
Pure CdO	0.2650	0.4590	0.0056	0.0022
300	0.2944	0.5099	0.0055	0.0017
350	0.2952	0.5113	0.0085	0.0041
400	0.2943	0.5097	0.0050	0.0014
450	0.2943	0.5097	0.0055	0.0017
500	0.2947	0.5104	0.0047	0.0012
550	0.2954	0.5117	0.0050	0.0014

4.4.2 Photoluminescence Analysis

Photoluminescence spectroscopy was used to examine the defects, charge dynamics, and recombination processes in semiconductor nanoparticles. Figure 4.13 (a) shows the PL spectra for calcined pure and Sn-doped CdO nanoparticles, and Figure 4.13 (b) shows PL deconvolution of the samples calcined at a range of temperatures using UV excitation between 390 and 540 nm at an excitation wavelength of 320 nm.

The main emission of peaks, which is mainly found in the blue visible part (around 460–475 nm), is attributed to the recombination of electrons and holes via either intrinsic or extrinsic defects within the band gap. Pure CdO had the highest PL intensity centered at 464.83 nm, whereas the PL intensity decreased among the Sn-doped CdO samples, indicating suppression of radiative recombination due to Sn doping and improved charge separation (Nabi *et al.,* 2024). Figure 4.13 shows the PL spectra for calcined pure and Sn-doped CdO nanoparticles, and PL deconvolution for calcined samples.

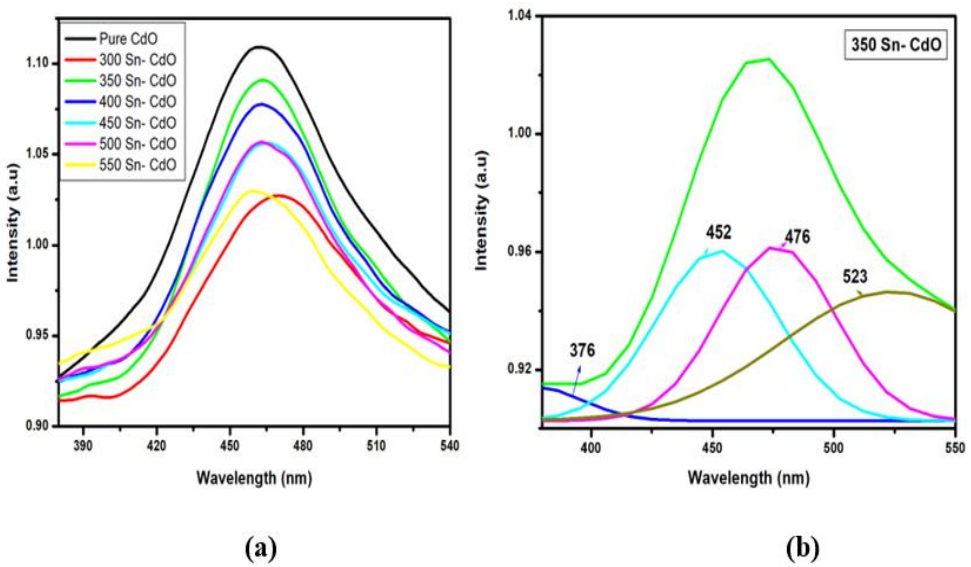


Figure 4.13: PL spectra showing Sn- CdO NPs calcined at different temperatures (a) and Gaussian deconvolution at 350 0C (b)

Interestingly, different levels of PL intensity were observed depending on the calcination temperature. The sample treated at 350°C had a secondary peak intensity of 0.16466 a.u., as shown in Table 4.11, indicating that defect states are strongly present even after doping with Sn. The smallest recombination was reported for the sample doped with 550°C tin at 0.09670 a.u., suggesting improved crystallinity and a decrease in interface traps. These findings reveal that moderately calcined crystals at temperatures of 400–550°C improve their overall structure and optoelectronic performance in solar cells. Gaussian deconvolution analysis of revealed multiple emission peaks at 376, 452, 476, and 523 nm. At 376 nm, near band edge (NBE) emission occurs, most likely due to free exciton recombination. Emissions at 452 and 476 nm are connected to oxygen vacancies and interstitials commonly found in CdO materials (Abbas *et al.*, 2021). At 523 nm, there is green emission attributed to the deep-level defects, including cadmium interstitials or states introduced by tin. When multiple visible-region emissions are displayed, it means that different degrees of defects are present, particularly at lower calcination temperatures where incomplete crystallization can trap charge carriers. This supports the greater dislocation count and lattice disarrangement found during XRD at 350°C. It is notable that PL intensity is generally reduced as the calcination process is taken from 300°C to 550°C, except for a small rise at 350°C. It shows that when the temperature for calcination is raised,

more grain growth occurs and the number of surface defects declines, decreasing the proportion of radiative recombination (Zhao *et al.,* 2022). A weaker PL means it is easier for photovoltaic applications to separate photo-generated carriers and avoid recombination phenomena (Makori *et al.,* 2014). These findings match other reports, for example, (Abbas *et al.,* 2021) found similar blue emission in CdO nanoparticles and noted that the PL intensity decreased as calcination temperature increased. In another study, (Vigil-Galán *et al.,* 2006) found that when Sn-doped CdO Nps were calcined above 450°C, the PL intensity decreased due to better grain linking and fewer trap states. Table 4.11 shows the emission wavelengths and relative intensities of peaks at varying calcination temperatures.

Table 4.11: Emission wavelengths and relative intensities of peaks at varying calcination temperatures

Calcination Temperature of Sn-CdO NPs (^{0}C)	**Emission Wavelength (nm)**	**Relative Intensity (a.u)**
Pure CdO	464.83	0.17549
300	475.67	0.10972
350	468.61	0.16466
400	468.08	0.14716
450	469.83	0.12296
500	467.43	0.12721
550	463.42	0.09670

4.4.3 FTIR Analysis

FTIR spectroscopy was used to examine the various vibrations and types of bonds within pure and Sn-doped CdO nanoparticles after being calcinated at different temperatures. All spectra measured in the range of 400–4000 cm^{-1}. Vibrational bands related to the structure and functional groups were examined to examine how varying calcination temperatures influenced the synthesized materials. The FTIR spectra is shown in Figure 4.14.

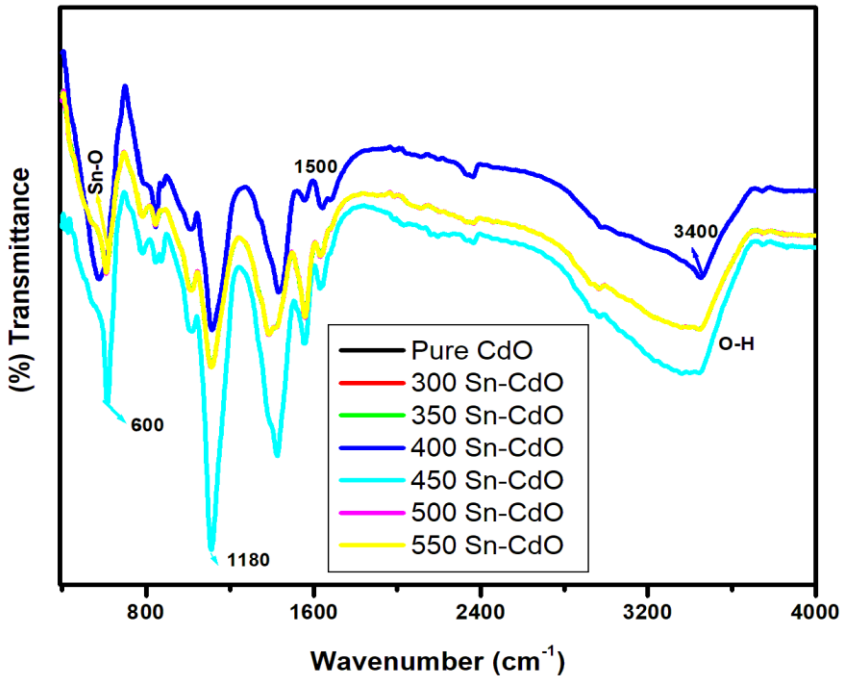


Figure 4.14: FTIR spectra of Sn- CdO NPs at different calcination temperatures

A major band between 3400 and 3600 cm^{-1} was seen in all synthesized samples and is commonly associated with O–H bond stretching of adsorbed water or available surface hydroxyl groups (Abbas *et al.,* 2021). The band's intensity at 300°C and 350°C shows that water from the surface is likely present due to incompletely removed water. As the calcination temperature increases, the strength of the band decreases, indicating that moisture and volatile organics are being effectively removed. The absorption band around 1400–1650 cm^{-1} is caused by the bending of water molecules or traces of organic molecules. The decreased intensity at 500°C and 550°C is attributed to the enhanced purity and densification of the oxide. Furthermore, the strong peaks noted below 700 cm^{-1}, mainly in the 450–650 cm^{-1} area, are attributed to the vibrations of single-crystal cadmium oxide (Makori *et al.,* 2014). The modified intensity of these peaks in the Sn-doped samples indicates that Sn^{4+} successfully replaced Cd^{2+}, which affects the bonding environment. The overlapping of Sn–O vibrations in this region may be seen in complex spectra of doped films, but are not always well-defined. When the calcination temperature increases, the FTIR spectra show clearer and sharper peaks, mainly at lower wavenumbers where the metal–oxygen bonds are located. This trend indicates a higher degree of crystallization and reduction of structural defects and precursor substances. From the results, the 500°C and 550°C samples show the

best consolidation, as they display less of the water-related bands and a more enhanced absorption of Cd by oxygen. These data support what was revealed in the XRD data, where the XRD patterns collected at 500°C displayed maximum crystallite sizes and the fewest defects, confirming the above observations. A similar behavior has been observed by (Makori *et al.,* 2014) found that exposing Sn-doped CdO thin NPs to temperatures above 450°C decreased the amount of carbon and improved the strength of the oxide network. In another study (Abbas *et al.,* 2021) also found a strong O–H bond in CdO nanoparticles synthesized by co-precipitation, and its intensity decreased as the nanoparticles were calcined at higher temperatures, indicating a higher-quality CdO phase. Sn impurity in CdO, studied by (Dakhel, 2011) led to a minor change in the Cd–O stretching band, resulting from shifts in the lattice and defect formation. The changes in FTIR spectra as the calcination temperature increases offer important clues about using Sn-doped CdO nanoparticles as photoanodes for solar cells. A lower intensity of hydroxyl and organic bands at high temperatures means the material is structurally pure and more suitable for efficient and less-reactive charge transfer. Also, the improved sharpness of Cd–O bands which indicates better crystallinity, as this is significant for producing defect-free materials useful in solar cells.

4.4.4 Optical Analysis

The ability of semiconducting materials to transmit and absorb light is crucial for their use in solar energy applications. The UV-Vis absorption and Tauc plot analyses were used to examine the optical transitions and determine the band gap energies of pure CdO and Sn-CdO NPs at varying calcination temperatures.

The absorbance spectra in Figure 4.15 at (200-900 nm) reveal a strong absorption in the ultraviolet region and the absorption edges shifts sharply depending on the calcination temperature and Sn doping. Pure CdO shows moderate absorption and a long tail, revealing that defects are present within its band gap. Samples doped with Sn, when calcined at 300°C and 350°C, exhibit increased absorption in the UV spectrum. The observed improvement is attributed to the development of Sn-based defects or by making the surface rougher, both of which help absorb more light (Abbas *et al.,* 2021). Beyond 400°C, the absorbance slightly decreases, possibly due to the development of a more uniform and uniformly colored crystal. At 500°C and 550°C, the samples display distinct absorption edges and fewer sub-band gaps, pointing to

less structural disorder and making them good choices for light harvesting in solar cells (De León-Gutiérrez *et al.,* 2006). The absorbance spectra of tin doped cadmium oxide is illustrated in figure 4.15

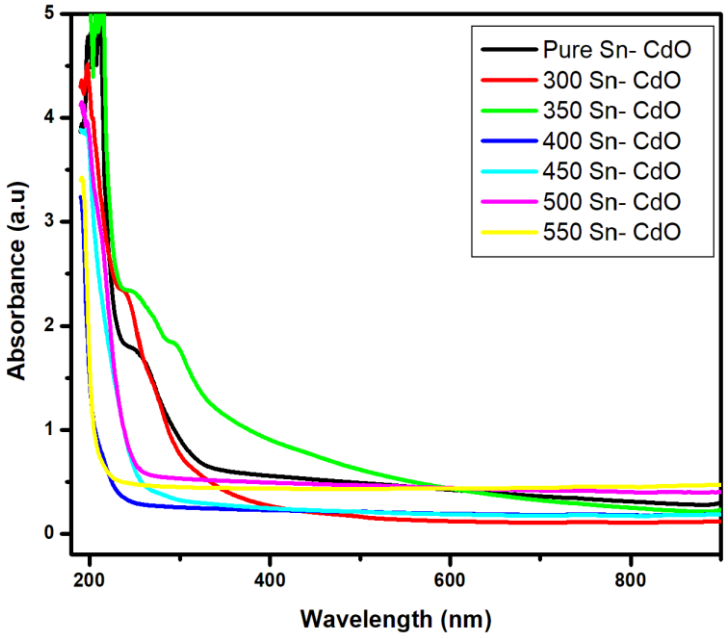


Figure 4.15: Absorbance spectra of Sn- CdO NPs calcined at different temperatures

To correctly estimate the band gap of pure CdO and CdO: Sn NPs, Tauc relation equation (Othman, 2022) was used. To obtain the bandgap energy from a Tauc's plot, the UV-Vis absorption spectrum of the sample was used to record the absorbance data, typically in the range of 200 to 800 nm. The absorbance data was then converted into photon energy (hν) using the equation $h\nu = \frac{1240}{\lambda}$ where λ is the wavelength in nanometres and hν is the photon energy in electron volts (eV). The absorption coefficient (α) was calculated, using the relation $\alpha = \frac{2.303\ X\ A}{t}$ where A is the absorbance and t is the thickness of the sample. The Tauc equation, was then applied, where E_g is the optical band gap and γ is 2 for indirect allowed transitions. A graph is plotted with hν on the x-axis and (αhν) on the y-axis. The linear portion of the curve near the absorption edge was extrapolated to intersect the x-axis. The point of intersection represents the band gap energy of the material.

$$(\alpha h\nu)^{\gamma} = Ah\nu - AE_g \qquad (4.10)$$

where α is the absorption coefficient, hv is the incident photon energy, γ is allowed transition, A is a constant and Eg is the electronic band gap of the semiconductor material. When γ is 2 it is indirect and when ½ it is direct allowed transition from the valence band to transition. Figure 4.16 shows the Tauc's plot.

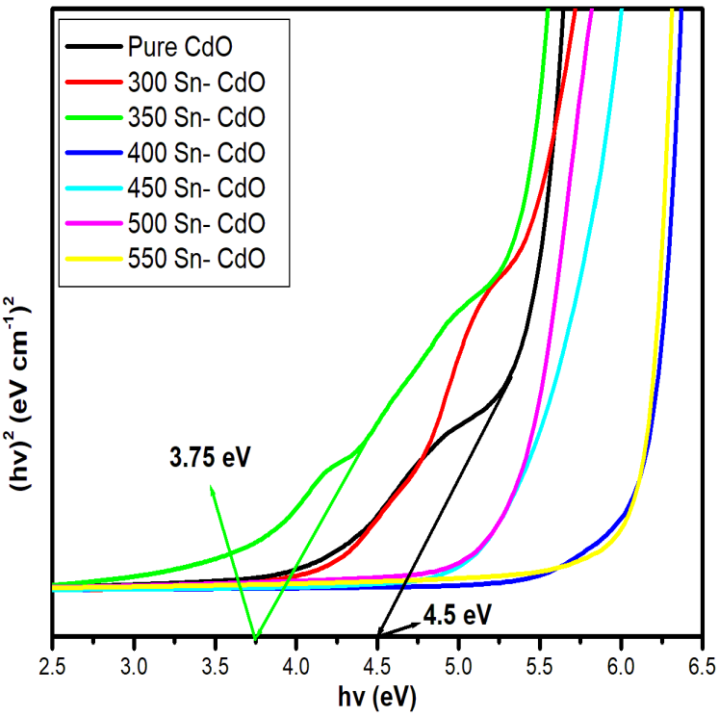


Figure 4.16: Tauc's plot and band of CdO: Sn NPs at different calcination temperatures

The band gap of pure CdO (4.50 eV) exceeds the typical regular bulk of CdO (~2.2–2.5 eV) dure to the quantum confinement effects in the nanoscale regime. (Makori *et al.,* 2014). Dopants in Sn typically push the gap between bands slightly wider at first, in line with the Burstein–Moss effect, as more carriers fill up the conduction band and the material's light absorption energy also increases (Gibbs *et al.,* 2013). Still, a major drop to 3.75 eV at 350°C likely results from the presence of disorder or defects due to incomplete crystallization or discrepancies in the doping process. Above 400°C as shown in Table 4.12, the band gap in the material becomes larger (up to 5.75 eV at 550°C) due to enhanced crystal structure, minimal defects, and potentially different conductivity (Abbas *et al.,* 2021). It is also observed that increasing the temperature during calcination made the band gap of CdO nanoparticles wider, matching the findings of (De León-Gutiérrez *et al.,* 2006), who observed that in Sn-doped CdO NPs,

the optical band gap increased from ~3.1 eV to ~5.1 eV due to the interplay of doping and thermal processing. The results of this work are important for solar cell engineering and design. The fact that thermal treatment and doping allow for fine-tuning the band gap from 3.7–5.75 eV is a major advantage when considering photovoltaics. A photoanode made of Sn-doped CdO blocks visible light from passing through, while injecting electrons into the conduction band. Table 4.12 shows the bandgaps of Sn doped cadmium oxide nanoparticles calcined at different temperature.

Table 4.12: Showing extrapolated bandgaps of Sn-CdO NPs at different calcination temperatures

Calcination Temperature of Sn-CdO NPs (^{0}C)	**Band gap (eV)**
Pure CdO	4.50
300	4.82
350	3.75
400	5.50
450	5.0
500	5.25
550	5.75

4.5 Chapter Summary

The single-phase cubic CdO (JCPDS No. 01-073-6494) and successful incorporation of Sn were confirmed when the XRD analysis showed no visible secondary phases. During calcination, the crystallite size increased until it reached a maximum of 27.98 nm at 500°C, and strain and dislocations in the structure were both reduced at that temperature. With higher calcination temperatures, FTIR spectra showed a gradual disappearance of hydroxyl groups and organic residue, accompanied by clearer bands for Cd-O stretching which indicates better crystallinity. Photoluminescence analysis showed broad blue emission associated with oxygen vacancies and defects, normalized and the PL intensity dropped with increasing calcination temperatures, showing that carrier recombination was less frequent. Optical analysis through UV-Vis spectroscopy and Tauc plots showed that the band gaps of the samples changed from 3.75 eV to 5.75 eV, with the sharpest absorption edge and largest gap appearing at 550°C, which was attributed to the Burstein–Moss effect and lower defect density. Based on the results, adjusting the calcination

temperature greatly affects the structure and performance of Sn-CdO nanoparticles in light-related applications. The study offers a useful way to improve CdO: Sn NPs for use in solar energy and optoelectronic applications in the future.

CHAPTER FIVE

CONCLUSION AND RECOMMENDATIONS

5.1 Conclusion

The pure and doped CdO NPs were successfully synthesized using a wet chemical process and then characterized using various techniques. XRD analysis confirmed a face-centered cubic structure of CdO for the experimental factors: capping ratio, doping concentration and calcination temperatures. The XRD pattern confirmed the retention of the cubic phase of CdO with no secondary phases when capped with MPA. The capping ratio greatly affected its quality and size of the crystallites. Using a moderate amount of MPA (1.5–2.0 ml) formed the best crystals with minimal defects and stress, since more MPA (2.5–3.0 ml) blocked crystal collisions and thus raised the number of defects in the crystals. The single-phase cubic CdO (JCPDS No. 01-073-6494) and successful incorporation of Sn were confirmed when the XRD analysis showed no visible secondary phases. During calcination, the crystallite size increased until it reached a maximum of 27.98 nm at 500°C, and strain and dislocations in the structure were both reduced at that temperature.

UV-Vis analysis revealed that addition of MPA to CdO, the optical band gaps shifted from 5.5 eV to as narrow as 3.5 eV, meaning the optical absorption behavior of these nanoparticles can be changed through proper choice of ligands. Absorbance of the nanoparticles increased with increasing Sn dopant in the range of 298nm to 340nm and their corresponding band gap energy decreased with increase in the dopant (3.688 eV to 1.812eV). Optical analysis through UV-Vis spectroscopy and Tauc plots showed that the band gaps of the samples changed from 3.75 eV to 5.75 eV, with the sharpest absorption edge and largest gap appearing at 550°C.

Mercaptopropionic acid (MPA) functional groups were successfully added, displaying unique vibrations from the Cd–O, C=O, O–H, and S–H groups. An increase in the intensity of carboxylate and thiol vibrations as more capping agent is added shows that the surface is being effectively modified and this changes the order and light response. Therefore, the research results indicate that changing the capping ratio on MPA leads to different CdO nanoparticles. Among the samples, 2 mL MPA-capped CdO revealed the best combination of properties, so it was the best for potential use in solar cell photoanodes. These findings advance the knowledge of making advanced

optoelectronic devices by engineering nanostructures using targeted molecules. With higher calcination temperatures, FTIR spectra showed a gradual disappearance of hydroxyl groups and organic residue, accompanied by clearer bands for Cd-O stretching which indicates better crystallinity.

The results from photoluminescence studies indicated that the intensity of PL depended non-linearly on capping concentration, and 2 ml MPA-capped sample gave stronger emission owing to effective passivation at the surface. Multiple defect-related emissions and emission near the band edge were clearly detected by Gaussian deconvolution. PL properties showed a decrease in peak intensity of the nanoparticles when doping was increased and a shift in emission wavelength from 395nm for pure to 400nm in doping with 3.5% Sn. The synthesized nanoparticles possessed good structural and optical properties for possible solar cell applications. Photoluminescence analysis of the calcined samples showed broad blue emission associated with oxygen vacancies and defects. It normalized and the PL intensity dropped with increasing calcination temperatures, showing that carrier recombination was less frequent.

The study also explored the impact of calcination temperature on the structural, and optical properties of tin-doped cadmium oxide (Sn-CdO) nanoparticles made using precipitation by reflux. The single-phase cubic CdO (JCPDS No. 01-073-6494) and successful incorporation of Sn were confirmed when the XRD analysis showed no visible secondary phases. During calcination, the crystallite size increased until it reached a maximum of 27.98 nm at 500°C, and strain and dislocations in the structure were both reduced at that temperature. With higher calcination temperatures, FTIR spectra showed a gradual disappearance of hydroxyl groups and organic residue, accompanied by clearer bands for Cd-O stretching which indicates better crystallinity. Photoluminescence analysis showed broad blue emission associated with oxygen vacancies and defects, normalized and the PL intensity dropped with increasing calcination temperatures, showing that carrier recombination was less frequent. Optical analysis through UV-Vis spectroscopy and Tauc plots showed that the band gaps of the samples changed from 3.75 eV to 5.75 eV, with the sharpest absorption edge and largest gap appearing at 550°C, which was attributed to the Burstein–Moss effect and lower defect density. Based on the results, adjusting the calcination

temperature greatly affects the structure and performance of Sn-CdO nanoparticles in light-related applications. These studies offer a useful way to improve Sn-CdO NPs for use in solar energy and optoelectronic applications in the future.

The research findings showed optimized results at 2ml MPA capping ratio, 1.5% tin doping concentration and calcination temperature 350 degrees Celsius for the nanoparticles synthesized using wet chemical process. The optimized parameters contribute to the development of sustainable and effective solar cell for utilization of renewable energy sources and global solution of energy crisis.

5.2 Recommendations

5.2.1 Recommendations for Policy

The study recommends the following for the optimized MPA capped cadmium oxide nanoparticles doped with tin (CdO: Sn) for possible solar cell application in order to improve its efficiency and enhance sustainable energy which is friendly to the environment;

- Best Synthesis Parameters of Solar Cells-The study recommends a capping ratio of 2mL MPA, 1.5%Sn doping and calcinating temperature of 350^0C to produce nanoparticles with optimal crystal tomography, minimum defect concentration and preferable optical band gap to make excellent solar cell photoanodes with efficiency.
- Cost-effective devices materials-Based on the foregoing parameters, the synthesized optimized particles of cadmium oxide (CdO) that result in low-cost but high-performance production of solar cells should be prioritized because of the stability of their structure, the tunability of optical properties, and scalable production process.

5.2.2 Recommendation for future work

Future work in the field of CdO: Sn nanoparticles for solar cell applications could focus on several key areas to advance the understanding and utilization of these materials:

- Explore alternative dopants – Investigate co-doping with other metals (e.g., In, Al, Ga) for improved DSSC efficiency.

- Investigation of other capping agents in synthesis of the nanoparticles for better quality of the photoanodes.
- Advance to device fabrication incorporating optimized cadmium oxide doped with tin nanoparticles.

REFERENCES

Aadim, K. A., Ahmed, B. M., & Khalaf, M. A. (2020). Influence of Sn doping ratio on the structural and optical properties of CdO films prepared by laser induced plasma. *Iraqi Journal of Physics*, *18*(45), 1–8. https://doi.org/10.30723/ijp.v18i45.523

Abbas, S., Basma, H., Al Boukhari, J., & Awad, R. (2021). Characterization of CdO nanoparticles prepared by co-precipitation method under different pH and calcination temperatures. *Applied Physics A*, *127*(7), 505. https://doi.org/10.1007/s00339-021-04669-5

Abid, I., Benzo, P., Pécassou, B., Jia, S., Zhang, J., Yuan, J., Dory, J. B., Gauthier Lafaye, O., Péchou, R., Mlayah, A., & Lou, J. (2021). Plasmon damping and charge transfer pathways in Au@MoSe2 nanostructures. *Materials Today Nano*, *15*, 100131. https://doi.org/10.1016/j.mtnano.2021.100131

Albin, D. S., Amarasinghe, M., Reese, M. O., Moseley, J., Moutinho, H., & Metzger, W. K. (2021). Colossal grain growth in Cd(Se,Te) thin films and their subsequent use in CdTe epitaxy by close-spaced sublimation. *Journal of Physics: Energy*, *3*(2), 024003. https://doi.org/10.1088/2515-7655/abd297

Al-Hada, N. M., Saion, E. B., Shaari, A. H., Kamarudeen, M. A., Flaifel, M. H., & Gene, S. A. (2015). Synthesis, Structural and Morphological Properties of Cadmium Oxide Nanoparticles Prepared by Thermal Treatment Method. *Advanced Materials Research*, *1107*, 291–294. https://doi.org/10.4028/www.scientific.net/AMR.1107.291

Anitha, M., Saravanakumar, K., Anitha, N., Kulandaisamy, I., & Amalraj, L. (2019). Influence of annealing temperature on physical properties of Sn-doped CdO thin films by nebulized spray pyrolysis technique. *Materials Science and Engineering: B*, *243*, 54–64. https://doi.org/10.1016/j.mseb.2019.03.018

Azzaoui, W., Medles, M., Salim, K., Nakrela, A., Bouzidi, A., Miloua, R., Amroun, M. N., & Khadraoui, M. (2023). Characterization and physical property studies of Sn, Al doped and co-doped CdO thin films. *Revista Mexicana de Física*, *69*(1 Jan-Feb). https://doi.org/10.31349/RevMexFis.69.011002

Baishya, K., Ray, J. S., Dutta, P., Das, P. P., & Das, S. K. (2018). Graphene-mediated band gap engineering of WO3 nanoparticle and a relook at Tauc equation for band gap evaluation. *Applied Physics A*, *124*(10), 704. https://doi.org/10.1007/s00339-018-2097-0

Bansal, A. K. (2019). Research Paper on Advanced Material used in Solar Panel—Perovskite, A organic, Inorganic and Halide Compound. *International Journal of Mechanical Engineering*, *6*(6), 48–55. https://doi.org/10.14445/23488360/IJME-V6I6P109

Bekele, E. T., & Sintayehu, Y. D. (2022). Recent Progress, Advancements, and Efficiency Improvement Techniques of Natural Plant Pigment-Based Photosensitizers for Dye-Sensitized Solar Cells. *Journal of Nanomaterials*, *2022*(1), 1024100. https://doi.org/10.1155/2022/1024100

Bett, K., Kiprotich, S., Ungula, J., & Andayi, W. (2024). Structural and Optical Properties of ZnO:Al:Ga Co-Doped Nanoparticles: Investigation on the Effects of pH of the Precursor Solution via a Simple Sol-Gel Route. *American Journal of Materials Science*, *14*(2), 21–30.

Bhosale, A. S., Abitkar, K. K., Sadalage, P. S., Pawar, K. D., & Garadkar, K. M. (2021). Photocatalytic and antibacterial activities of ZnO nanoparticles synthesized by chemical method. *Journal of Materials Science: Materials in Electronics*, *32*(15), 20510–20524. https://doi.org/10.1007/s10854-021-06563-5

Bunaciu, A. A., Udriştioiu, E. G., & Aboul-Enein, H. Y. (2015). X-Ray Diffraction: Instrumentation and Applications. *Critical Reviews in Analytical Chemistry*, *45*(4), 289–299. https://doi.org/10.1080/10408347.2014.949616

Contreras-Rascón, J. I., Díaz-Reyes, J., Flores-Pacheco, A., Serrano-de La Rosa, L. E., Del Ángel-Vicente, P., Lozada Morales, R., Álvarez Ramos, M. E., & López-Salazar, P. (2020). Enhanced photoluminescence effects in nanostructured cubic CdS matrix doped with Cu2+ obtained by chemical Bath deposition. *Journal of Materials Research and Technology*, *9*(1), 364–372. https://doi.org/10.1016/j.jmrt.2019.10.065

Dakhel, A. A. (2011). Effect of cerium doping on the structural and optoelectrical properties of CdO nanocrystallite thin films. *Materials Chemistry and Physics*, *130*(1–2), 398–402. https://doi.org/10.1016/j.matchemphys.2011.06.060

Dasuki, D., Habanjar, K., & Awad, R. (2023). Effect of Growth and Calcination Temperatures on the Optical Properties of Ruthenium-Doped ZnO Nanoparticles. *Condensed Matter*, *8*(4), 102. https://doi.org/10.3390/condmat8040102

De León-Gutiérrez, L. R., Cayente-Romero, J. J., Peza-Tapia, J. M., Barrera-Calva, E., Martínez-Flores, J. C., & Ortega-López, M. (2006). Some physical properties of Sn-doped CdO thin films prepared by chemical bath deposition. *Materials Letters*, *60*(29–30), 3866–3870. https://doi.org/10.1016/j.matlet.2006.03.131

Ellerbrock, R. H., & Gerke, H. H. (2021). FTIR spectral band shifts explained by OM–cation interactions. *Journal of Plant Nutrition and Soil Science*, *184*(3), 388–397. https://doi.org/10.1002/jpln.202100056

Fall, A., Sackey, J., Mayedwa, N., & Ngom, B. D. (2021). Investigation of structural and optical properties of CdO nanoparticles via peel of Citrus x sinensis. *Materials Today: Proceedings*, *36*, 298–302. https://doi.org/10.1016/j.matpr.2020.04.057

Gary Kwok, C. K., Liu, C. P., & Yu, K. M. (2019). Sol-gel synthesis of highly transparent and conducting Cadmium Oxide. *2019 Compound Semiconductor Week (CSW)*, 1–2. https://doi.org/10.1109/ICIPRM.2019.8819192

Gibbs, Z. M., LaLonde, A., & Snyder, G. J. (2013). Optical band gap and the Burstein–Moss effect in iodine doped PbTe using diffuse reflectance infrared Fourier transform spectroscopy. *New Journal of Physics*, *15*(7), 075020. https://doi.org/10.1088/1367-2630/15/7/075020

Green, M. A., Dunlop, E. D., Hohl-Ebinger, J., Yoshita, M., Kopidakis, N., Bothe, K., Hinken, D., Rauer, M., & Hao, X. (2022). Solar cell efficiency tables (Version 60). *Progress in Photovoltaics: Research and Applications*, *30*(7), 687–701. https://doi.org/10.1002/pip.3595

Ikram, S., Ashraf, F., Alzaid, M., Mahmood, K., Amin, N., & Haider, S. A. (2021). Role of Nature of Rare Earth Ion Dopants on Structural, Spectral, and Magnetic Properties in Spinel Ferrites. *Journal of Superconductivity and Novel Magnetism*, *34*(7), 1745–1751. https://doi.org/10.1007/s10948-020-05723-8

Ivchenko, V. (2024). Theory of Burstein-Moss effect in semiconductors with anisotropic energy bands. *Physica Scripta*, *99*(3), 035952. https://doi.org/10.1088/1402-4896/ad28e5

Javed, R., Zia, M., Naz, S., Aisida, S. O., Ain, N. U., & Ao, Q. (2020). Role of capping agents in the application of nanoparticles in biomedicine and environmental remediation: Recent trends and future prospects. *Journal of Nanobiotechnology*, *18*(1), 172. https://doi.org/10.1186/s12951-020-00704-4

Jiang, J., Pi, J., & Cai, J. (2018). The Advancing of Zinc Oxide Nanoparticles for Biomedical Applications. *Bioinorganic Chemistry and Applications*, *2018*, 1062562. https://doi.org/10.1155/2018/1062562

Kaliramna, S., Dhayal, S. S., Chaudhary, R., Khaturia, S., Ameta, K. L., & Kumar, N. (2022). A Review And Comparative Analysis Of Different Types Of Dyes For Applications In Dye-Sensitized Solar Cells. *Brazilian Journal of Physics*, *52*(4), 136. https://doi.org/10.1007/s13538-022-01109-4

Kamkird, P., Ketjoy, N., Rakwichian, W., & Sukchai, S. (2012). Investigation on Temperature Coefficients of Three Types Photovoltaic Module Technologies under Thailand Operating Condition. *Procedia Engineering*, *32*, 376–383. https://doi.org/10.1016/j.proeng.2012.01.1282

Karim, I., Naeem, M. A. H., Ayon, A. S. R., Sattar, Md. A., Sabur, Md. A., & Ahmed, A. N. (2025). Effect of silver and cobalt on transparent conducting CdO thin films: Tuning the optoelectronic properties. *Materials Advances*, *6*(2), 703–718. https://doi.org/10.1039/D4MA00918E

Kathalingam, A., Kesavan, K., Rana, A. U. H. S., Jeon, J., & Kim, H.-S. (2018). Analysis of Sn Concentration Effect on Morphological, Optical, Electrical and Photonic Properties of Spray-Coated Sn-Doped CdO Thin Films. *Coatings*, *8*(5), 167. https://doi.org/10.3390/coatings8050167

Kim, J. H., Cho, S. C., Hong, Y. C., & Uhm, H. S. (2007). Oxide Nanoparticles Synthesized in a Microwave Plasma Torch. *2007 IEEE Pulsed Power Plasma Science Conference*, 898–898. https://doi.org/10.1109/PPPS.2007.4346204

Kiprotich, S., Dejene, F. B., & Onani, M. O. (2022a). Effects of growth time on the material properties of CdTe/CdSe core/shell nanoparticles prepared by a facile wet chemical route. *Materials Research Express*, *9*(2), 025008. https://doi.org/10.1088/2053-1591/ac5073

Kiprotich, S., Dejene, F. B., & Onani, M. O. (2022b). Effects of growth time on the material properties of CdTe/CdSe core/shell nanoparticles prepared by a facile wet chemical route. *Materials Research Express*, *9*(2), 025008. https://doi.org/10.1088/2053-1591/ac5073

Langat, V. K., Kanali, C. L., Ronoh, E. K., Ondimu, S. N., Ndirangu, S. N., Roskilly, T., Royapoor, M., & Laidler, P. (2022). Effect of tilt angle on the performance of a thin-film photovoltaic system. *Journal of Agriculture, Science and Technology*, *21*(2), 96–104. https://doi.org/10.4314/jagst.v21i2.8

Latha, Ch. K., Raghasudha, M., Aparna, Y., M, Ramchander., Ravinder, D., K, Jaipal., Veerasomaiah, P., & Shridhar, D. (2017). Effect of Capping Agent on the Morphology, Size and Optical Properties of In2O3 Nanoparticles. *Materials Research*, *20*(1), 256–263. https://doi.org/10.1590/1980-5373-mr-2016-0292

Lathouwers, C., Singh, V., & Rajaputra, S. (2013). Nano-structured Cadmium Sulfide thin films for solar cell applications. *2013 Proceedings of IEEE Southeastcon*, 1–8. https://doi.org/10.1109/SECON.2013.6567442

L.C. Passos, M., & M.F.S. Saraiva, M. L. (2019). Detection in UV-visible spectrophotometry: Detectors, detection systems, and detection strategies. *Measurement*, *135*, 896–904. https://doi.org/10.1016/j.measurement.2018.12.045

Lee, K. M., Park, K. H., Koh, K. H., & Lee, S. (2007). Synthesis of High Quality ZnO Nanorods by Low Temperature Wet Chemical Process. *2007 2nd IEEE International Conference on Nano/Micro Engineered and Molecular Systems*, 775–778. https://doi.org/10.1109/NEMS.2007.352132

Li, M., & Li, J. C. (2006). Size effects on the band-gap of semiconductor compounds. *Materials Letters*, *60*(20), 2526–2529. https://doi.org/10.1016/j.matlet.2006.01.032

Lu, K. (2023). Comparison and Evaluation of Different Types of Solar Cells. *Applied and Computational Engineering*, *23*(1), 263–270. https://doi.org/10.54254/2755-2721/23/20230664

Makori, N. E., Amatalo, I. A., Karimi, P. M., & Njoroge, W. K. (2014). *Optical and electrical properties of CdO: Sn thin films for solar cell applications*. http://ir-library.ku.ac.ke/handle/123456789/14849

Mandal, S., Ali, S. I., Pramanik, S., & Mandal, A. C. (2023). *Impact of capping agent on structural and optical properties of ZnS nanoparticles* (Version 1). arXiv. https://doi.org/10.48550/ARXIV.2304.13420

Mazhar, A., Elkholy, N. S., Yousif, N. M., & Shalaby, M. S. (2023). Investigations of Structural, Optical, Thermal, and spectroscopic characteristics of CdO-Ni nanoparticles employed in anti-cancer activities for cancer cells. *Results in Chemistry*, *6*, 101204. https://doi.org/10.1016/j.rechem.2023.101204

Mohamed, M. A., Jaafar, J., Ismail, A. F., Othman, M. H. D., & Rahman, M. A. (2017). Fourier Transform Infrared (FTIR) Spectroscopy. In *Membrane Characterization* (pp. 3–29). Elsevier. https://doi.org/10.1016/B978-0-444-63776-5.00001-2

Mohammad Bagher, A. (2015). Types of Solar Cells and Application. *American Journal of Optics and Photonics*, *3*(5), 94. https://doi.org/10.11648/j.ajop.20150305.17

Mohd Raub, A. A., Bahru, R., Mohd Nashruddin, S. N. A., & Yunas, J. (2024). Advances of nanostructured metal oxide as photoanode in photoelectrochemical (PEC) water splitting application. *Heliyon*, *10*(20), e39079. https://doi.org/10.1016/j.heliyon.2024.e39079

Morris, K. M., Togay, M., Jones, L., Walls, J. M., & Bowers, J. W. (2023). Co-Sputtered Sn-Doped ZnO Thin Film n-Type Layers for Incorporation into CdTe Based Photovoltaics. *2023 IEEE 50th Photovoltaic Specialists*

Conference (PVSC), 1–6. https://doi.org/10.1109/PVSC48320.2023.10359899

Nabi, G., Riaz, A., Dahshan, A., Tanveer, M., Maraj, M., & Ali, W. (2024). Sn doping role in structural modifications and electrochemical performance of Co(OH)2 nanorods for supercapacitors applications. *Materials Chemistry and Physics*, *314*, 128944. https://doi.org/10.1016/j.matchemphys.2024.128944

Nasir, E. M., Naji, I. S., & Alias, M. F. A. (2013). *Characterization of Cadmium Tin Oxide Thin Films as a Window Layer for Solar Cell*. *2*(9).

Nelson, H. D., Li, X., & Gamelin, D. R. (2016). Computational Studies of the Electronic Structures of Copper-Doped CdSe Nanocrystals: Oxidation States, Jahn–Teller Distortions, Vibronic Bandshapes, and Singlet–Triplet Splittings. *The Journal of Physical Chemistry C*, *120*(10), 5714–5723. https://doi.org/10.1021/acs.jpcc.5b11319

Othman, M. (2022). Optical Characteristics of Cadmium Oxide and Magnesium Doped with Nanoclusters. *ECS Journal of Solid State Science and Technology*, *11*(1), 013012. https://doi.org/10.1149/2162-8777/ac4c7e

Pattabi, M. (2003). The effect of precursor concentration on the size of the CdS nanoparticles synthesized in a chicken egg membrane. *Solar Energy Materials and Solar Cells*, *76*(3), 323–330. https://doi.org/10.1016/S0927-0248(02)00284-2

Picollo, M., Aceto, M., & Vitorino, T. (2019). UV-Vis spectroscopy. *Physical Sciences Reviews*, *4*(4), 20180008. https://doi.org/10.1515/psr-2018-0008

Prakash, T., Kumar, E. R., Gnanamoorthi, K., Munshi, A. M., Almehmadi, S. J., Mersal, G. A. M., & El Metwaly, N. M. (2021). Evaluation of phase, morphological, optical and electrical properties of microwave synthesized Sn doped CdO nanostructures. *Solid State Communications*, *336*, 114388. https://doi.org/10.1016/j.ssc.2021.114388

Rahdar, A. (2013). Effect of 2-mercaptoethanol as capping agent on ZnS nanoparticles: Structural and optical characterization. *Journal of Nanostructure in Chemistry*, *3*(1), 10. https://doi.org/10.1186/2193-8865-3-10

Rathore, N., Panwar, N. L., Yettou, F., & Gama, A. (2021). A comprehensive review of different types of solar photovoltaic cells and their applications. *International Journal of Ambient Energy*, *42*(10), 1200–1217. https://doi.org/10.1080/01430750.2019.1592774

Samanta, P. K., Mandal, A. K., Mishra, S., & Saha, A. (2017). Wet-chemical synthesis and optical properties of CuO nanoparticles. *2017 1st International Conference on Electronics, Materials Engineering and Nano-Technology (IEMENTech)*, 1–3. https://doi.org/10.1109/IEMENTECH.2017.8076941

Seetawan, U., Jugsujinda, S., Seetawan, T., Euvananont, C., Junin, C., Thanachayanont, C., Chainaronk, P., & Amornkitbamrung, V. (2011). Effect of annealing temperature on the crystallography, particle size and thermopower of bulk ZnO. *Solid State Sciences*, *13*(8), 1599–1603. https://doi.org/10.1016/j.solidstatesciences.2011.06.007

Sharma, S., Jain, K. K., & Sharma, A. (2015). Solar Cells: In Research and Applications—A Review. *Materials Sciences and Applications*, *06*(12), 1145–1155. https://doi.org/10.4236/msa.2015.612113

Sharma, S., & Kapoor, A. (2016). Structural and optical studies of cadmium doped zinc oxide thin films for solar cells. *2016 3rd International Conference on Emerging Electronics (ICEE)*, 1–3. https://doi.org/10.1109/ICEmElec.2016.8074627

Sharma, V. K., Filip, J., Zboril, R., & Varma, R. S. (2015). Natural inorganic nanoparticles – formation, fate, and toxicity in the environment. *Chemical Society Reviews*, *44*(23), 8410–8423. https://doi.org/10.1039/C5CS00236B

Shen, X., Kang, K., Yu, Z., Jeong, W. H., Choi, H., Park, S. H., Stranks, S. D., Snaith, H. J., Friend, R. H., & Lee, B. R. (2023). Passivation strategies for mitigating defect challenges in halide perovskite light-emitting diodes. *Joule*, *7*(2), 272–308. https://doi.org/10.1016/j.joule.2023.01.008

Sidor, J. J. (2024). Quantitative Indicators of Microstructure and Texture Heterogeneity in Polycrystalline System. *Materials*, *17*(24), 6057. https://doi.org/10.3390/ma17246057

Sukanya, D., & Sagayaraj, P. (2015). *A simple and facile synthesis of MPA capped CdSe and CdSe/CdS core/shell nanoparticles*. 050028. https://doi.org/10.1063/1.4917669

Tala-Ighil, R. (2015). Nanomaterials in Solar Cells. In M. Aliofkhazraei & A. S. H. Makhlouf (Eds.), *Handbook of Nanoelectrochemistry* (pp. 1–18). Springer International Publishing. https://doi.org/10.1007/978-3-319-15207-3_26-1

Tin dopped cadmium oxide.pdf. (n.d.).

Udoka, M. E., Nnadozie, E. L., Ifeyinwa, O., & Livinus, O. N. (2020). *Synthesis and Characterization of Manganese Doped Cadmium Oxide Thin Films by Electrodeposition Method*. *4*(1).

Ullah, H., Rahaman, R., & Mahmud, S. (2017). Optical Properties of Cadmium Oxide (CdO) Thin Films. *Indonesian Journal of Electrical Engineering and Computer Science*, *5*(1), 81. https://doi.org/10.11591/ijeecs.v5.i1.pp81-84

Vernon-Parry, K. D. (2000). Scanning electron microscopy: An introduction. *III-Vs Review*, *13*(4), 40–44. https://doi.org/10.1016/S0961-1290(00)80006-X

Vigil-Galán, O., Sánchez-González, Y., Arias-Carbajal, A., Contreras-Puente, G., Tufiño-Velázquez, M., & Ruiz, C. M. (2006). Influence of Sn concentration on the physical properties of CdO:Sn thin films deposited by spray pyrolysis. *Physica Status Solidi (a)*, *203*(15), 3713–3719. https://doi.org/10.1002/pssa.200521500

Wageh, S. (2014). Light Emitting Devices Based on CdSe Nanoparticles Capped With Mercaptoacetic Acid. *IEEE Journal of Quantum Electronics*, *50*(9), 1–8. https://doi.org/10.1109/JQE.2014.2335819

Wiengnon, S., & Anuragudom, P. (2019). Synthesis, and characterization of Iron-doped Zinc Oxide nanoparticles; Influence of drying. *Materials Today: Proceedings*, *17*, 1479–1486. https://doi.org/10.1016/j.matpr.2019.06.171

Yang, W., Cai, Y., Cai, H., Gu, C., Xu, W., Huang, W., & Yang, W. (2025). Fluorescent turn-off-on aptasensors with CdZnTe quantum dots and MoS2 nanosheets for highly sensitive detection of sulfadiazine residues.

Microchemical Journal, *212*, 113536. https://doi.org/10.1016/j.microc.2025.113536

Zak, A. K., Abrishami, M. E., Majid, W. A., Yousefi, R., & Hosseini, S. M. (2011). Effects of annealing temperature on some structural and optical properties of ZnO nanoparticles prepared by a modified sol–gel combustion method. *Ceramics International*, *37*(1), 393–398.

Zhang Jin-Li, Li Biao-Rong, & Jin Qi-Lu. (1989). The structure, phase transformation and electrical properties of a new cadmium antimony oxide semiconductive ceramics. *Proceedings., 39th Electronic Components Conference*, 909–912. https://doi.org/10.1109/ECC.1989.77855

Zhang, Y., Zhang, H., Ma, M., Guo, X., & Wang, H. (2009). The influence of ligands on the preparation and optical properties of water-soluble CdTe quantum dots. *Applied Surface Science*, *255*(9), 4747–4753. https://doi.org/10.1016/j.apsusc.2008.09.009

Zhao, Y., Xu, L., Guo, M., Li, Z., Xu, Z., Ye, J., Li, W., & Wei, S. (2022). Effects of calcination temperature on grain growth and phase transformation of nano-zirconia with different crystal forms prepared by hydrothermal method. *Journal of Materials Research and Technology*, *19*, 4003–4017. https://doi.org/10.1016/j.jmrt.2022.06.137

Zhenguo Ji, Yueteng Yao, Junhua Xi, & Qiuhong Wu. (2011). Deposition of transparent conducting CdO on flexible PET substrate. *2011 International Conference on Multimedia Technology*, 5799–5802. https://doi.org/10.1109/ICMT.2011.6002355

APPENDICES

Appendix 1: Approval letter

MURANG'A UNIVERSITY OF TECHNOLOGY

Office of the Director, Postgraduate Studies

E-mail: [illegible]
Website: www.mut.ac.ke

P.O. Box 75-10200
Murang'a, Kenya

Ref: MUT/ARP/PGS/19/2020 /VOL.1 **Date:** 12th February, 2025

Ms. Jepchumba Nancy Kiprotich – AS402/5108/2023

School of Pure, Applied and Health Sciences,
Murang'a University of Technology,
P.O. Box 75-10200
Murang'a.

Dear Ms. Kiprotich,

RE: APPROVAL OF RESEARCH PROPOSAL AND SUPERVISORS.

I am pleased to inform you that the Directorate of Postgraduate Studies on 10th February 2025 considered and approved your Master research proposal entitled ***"Synthesis and Characterization of Tin Doped Cadmium Oxide Nano particles for possible solar cell Application."*** and appointed the following as supervisors:- Murang'a University of Technology

1. Dr. John Njagi - Murang'a University of Technology
2. Dr. Peter Waithaka - Murang'a University of Technology

You may now proceed with your data collection subject to obtaining research permit from NACOSTI, if required. You should also begin consulting your supervisors and submit through them quarterly progress reports to the Director Postgraduate Studies through your CoD and School Dean. Progress Reports forms can be accessed in the Student Portal.

It is the policy and regulations of the University that you observe deadlines. The guidelines on Postgraduate supervision can be accessed in the post graduate Handbook.

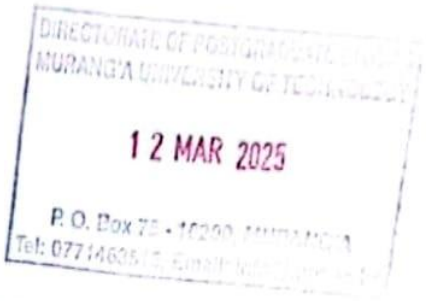
Your responsibilities as a student will include, among others;

i. Maintain regular consultation with your supervisor(s), at least once a month
ii. Submit quarterly reports on time, through your supervisors, CoD, Dean and to the Director of Postgraduate Studies;
iii. Ensure quality work all through;
iv. Present your research findings at 2-3 seminars/conferences prior to thesis examination.
v. Publish one article from your research findings in a refereed journal prior to thesis examination.

For any further clarification please contact the undersigned.

Yours Sincerely,

Prof. Geoffrey Muchiri, PhD
Director, Postgraduate Studies
GM/MM



Copy to:
1. Registrar – Academics and Students Affairs
2. Dean, School of Pure, Applied and Health Sciences

Appendix 2: Publications

This thesis has produced the following publication:

Kiprotich, N., Waithaka, P., Kiprotich, S., & Njagi, J. (2025). Effects of Tin Doping Concentration on the Structural and Optical Properties of Cadmium Oxide Nanoparticles. *Advances in Materials*, *14*(2), 55–64. https://doi.org/10.11648/j.am.20251402.13